



Article

Bio-Optical Properties and Ocean Colour Satellite Retrieval along the Coastal Waters of the Western Iberian Coast (WIC)

Luciane Favareto ^{1,2,*} , Natalia Rudorff ³ , Vanda Brotas ^{1,2} , Andreia Tracana ^{1,2}, Carolina Sá ⁴, Carla Palma ⁵ and Ana C. Brito ^{1,2}

¹ MARE—Marine and Environmental Sciences Centre, Faculdade de Ciências, Universidade de Lisboa, Campo Grande 16, 1749-016 Lisbon, Portugal

² Departamento de Biologia Vegetal, Faculdade de Ciências, Universidade de Lisboa, Campo Grande 16, 1749-016 Lisbon, Portugal

³ INPE—Instituto Nacional de Pesquisas Espaciais, Divisão de Satélites e Sistemas Ambientais, Rod. Presidente Dutra, Cachoeira Paulista 12630-000, SP, Brazil

⁴ Portugal Space, Estrada das Laranjeiras, 1500-423 Lisbon, Portugal

⁵ Instituto Hidrográfico, Rua das Trinas 49, 1249-093 Lisbon, Portugal

* Correspondence: lrfavareto@fc.ul.pt

Abstract: Essential Climate Variables (ECVs) like ocean colour provide crucial information on the Optically Active Constituents (OACs) of seawater, such as phytoplankton, non-algal particles, and coloured dissolved organic matter (CDOM). The challenge in estimating these constituents through remote sensing is in accurately distinguishing and quantifying optical and biogeochemical properties, e.g., absorption coefficients and the concentration of chlorophyll *a* (Chl*a*), especially in complex waters. This study evaluated the temporal and spatial variability of bio-optical properties in the coastal waters of the Western Iberian Coast (WIC), contributing to the assessment of satellite retrievals. In situ data from three oceanographic cruises conducted in 2019–2020 across different seasons were analyzed. Field-measured biogenic light absorption coefficients were compared to satellite estimates from Ocean-Colour Climate Change Initiative (OC-CCI) reflectance data using semi-analytical approaches (QAA, GSM, GIOP). Key findings indicate substantial variability in bio-optical properties across different seasons and regions. New bio-optical coefficients improved satellite data retrieval, reducing uncertainties and providing more reliable phytoplankton absorption estimates. These results highlight the need for region-specific algorithms to accurately capture the unique optical characteristics of coastal waters. Improved comprehension of bio-optical variability and retrieval techniques offers valuable insights for future research and coastal environment monitoring using satellite ocean colour data.



Citation: Favareto, L.; Rudorff, N.; Brotas, V.; Tracana, A.; Sá, C.; Palma, C.; Brito, A.C. Bio-Optical Properties and Ocean Colour Satellite Retrieval along the Coastal Waters of the Western Iberian Coast (WIC). *Remote Sens.* **2024**, *16*, 3440. <https://doi.org/10.3390/rs16183440>

Academic Editors: Andrew Clive Banks, Jason Keith Jolliff and Peng Chen

Received: 6 August 2024

Revised: 7 September 2024

Accepted: 9 September 2024

Published: 16 September 2024



Copyright: © 2024 by the authors. Licensee MDPI, Basel, Switzerland. This article is an open access article distributed under the terms and conditions of the Creative Commons Attribution (CC BY) license (<https://creativecommons.org/licenses/by/4.0/>).

Keywords: absorption coefficients; coloured dissolved organic matter—CDOM; detritus; chlorophyll *a* concentration; semi-analytical algorithms; Ocean-Colour Climate Change Initiative (OC-CCI)

1. Introduction

Ocean colour has been recognized as an Essential Climate Variable (ECV) by the Global Climate Observing System (GCOS, [1,2]). The term “ocean colour” refers to the residual spectrum of incident solar radiation that is constituted by the frequencies that emerge from the upper layer of the ocean after the incident radiation has been scattered and absorbed [3]. Ocean colour is therefore the result of this dispersion and absorption, as light interacts with the water and the materials in it, either particulates or dissolved, namely Optically Active Constituents (OACs). Specifically, in the visible range, passive radiometric sensors provide data on the Apparent Optical Properties (AOPs, e.g., surface reflectance) of the ocean to model the Inherent Optical Properties (IOPs) that depend on the OACs present in a given body of water [4]. The challenge in estimating these constituents through remote sensing is in accurately distinguishing and quantifying their IOPs and biogeochemical properties, e.g.,

the absorption coefficients of phytoplankton (a_{ph}), non-algal particles (NAPs or detritus, a_d), coloured dissolved organic matter (CDOM, a_g), and the concentration of chlorophyll *a* (Chl*a*).

After corrections for the atmospheric and unwanted surface effects (i.e., sun and sky glint and whitecaps), the accuracy of the retrieved water properties will depend on the proportion, interaction, type, and vertical distribution of the dissolved (fulvic and humic CDOM) and suspended particulate materials (i.e., organic and inorganic detritus and phytoplankton cells) [5]. Thus, before applying inversion ocean colour algorithms, it is necessary to understand and characterize the IOPs and the physics of the environment, which govern their distribution spatially and temporally. In coastal waters, IOPs and physicochemical properties are more variable on small scales of time and space compared to the open ocean. Freshwater inputs to the system are a source of particulate matter and dissolved organics, often influencing coastal stratification and hydrodynamics. In addition, there may be regions and seasons more subject to the action of wind and wave-induced bottom resuspension and coastal upwelling, where productivity and biological diversity are usually higher [6].

In waters where there is an optical dominance of phytoplankton absorption in the total absorption and where the other constituents, i.e., non-algal particles and CDOM, covary with Chl*a* (i.e., the product of phytoplankton degradation), the estimates of their bio-optical properties tend to be more precise. This is the case for predominantly oceanic waters, where Chl*a* is normally the dominant optical constituent, classified as Case 1 waters [7]. On the other hand, when the optical properties are influenced by the presence of particulate and dissolved materials that do not covary with phytoplankton, Case 2 waters, there is a greater complexity in estimating each of the IOPs [8], and this is when ocean colour algorithms tend to fail or present higher uncertainties.

Biogenic light absorption is a main optical property that can be used to identify phytoplankton based on their spectral characteristics (e.g., [9–13]), which is extremely valuable for addressing several issues like carbon cycling, fisheries management, and climate change [14,15]. Therefore, the characterization of the OACs and IOPs in coastal regions is an important step in determining the appropriate use of ocean-colour bio-optical algorithms, as well as their uncertainties [16] and the need for regional parametrizations of global models [17].

The Western Iberian Coast (WIC) is a highly dynamic region, seasonally influenced by coastal upwelling [18,19], as well as by continental river runoff and occasional storms [20]. The WIC's primary oceanographic features include the Iberian Poleward Current (IPC), upwelling jet, associated filaments, eddies, and the Western Iberian Buoyant Plume (WIBP). The upwelling system, shaped by the coast's morphology and wind patterns, exhibits high variability, particularly in the northern WIC (e.g., [19,21,22]). Nutrient inputs from continental sources or intense upwelling support phytoplankton growth, mainly in the northern region (between latitudes 39.5 and 42° N) [22,23]. In contrast, the southern WIC experiences limited phytoplankton growth due to lower nutrient availability, except in the cape of Sagres [24].

The challenge in estimating OACs through remote sensing is in accurately distinguishing and quantifying their optical and biogeochemical properties, especially in complex waters, such as the ones in the Western Iberian Coast (WIC). Thus, the main aim of this study was to evaluate the temporal and spatial variability of bio-optical properties in the coastal waters of Portugal, contributing to the assessment of the best approaches for satellite retrievals. To achieve this, the following specific objectives were considered: (i) analyze the bio-optical composition of the WIC's coastal waters and classify them according to the general case 1 and case 2 classification scheme; (ii) analyze the temporal and spatial variation of absorption coefficients for phytoplankton, detritus, and CDOM in order to understand their dynamics and sources within the WIC; (iii) investigate the relationships between biogeochemical and bio-optical properties; and (iv) assess the best approaches to deriving bio-optical and biogeochemical properties using ocean colour remote sensing. This study contributes to a better understanding of the bio-optical variability of ocean

colour in the coastal shelf off Portugal, providing valuable information for future research and monitoring efforts.

2. Materials and Methods

2.1. Sampling Campaigns

Under the framework of the AQUIMAR project (<https://aquimar.hidrografico.pt/>, accessed on 10 November 2023), four oceanographic campaigns (AQ1 to AQ4) were performed (Table 1), covering five sampling areas (A, B, C, D, and E). See [22] for details of the sampling campaigns. This study uses data from AQ2 to AQ4, as no bio-optical data were collected during AQ1. The AQ2 campaign was carried out within the period between April and May 2019 (spring), AQ3 in October 2019 (autumn), and AQ4 between February and March 2020 (called early spring, given the phytoplankton growing season). A total of 125 bio-optical samples were obtained during these campaigns (Table 1; Figure 1).

Table 1. Details and number (N) of bio-optical (absorption) samples collected during the oceanographic campaigns of AQUIMAR (AQ1 to AQ4) in five areas (A, B, C, D and E).

	Autumn (AQ1) October 2018				Spring (AQ2) April/May 2019				Autumn (AQ3) October 2019				Early Spring (AQ4) February/March 2020			
	Area	Start date	End date	N	Area	Start date	End date	N	Area	Start date	End date	N	Area	Start date	End date	N
No absorption data	E	18/04	22/04	11	E	10/10	13/10	11	C	24/02	25/02	6				
	D	29/04	30/04	9	B	21/10	23/10	9	D	27/02	28/02	9				
	B	02/05	05/05	9	A	24/10	26/10	9	E	29/02	02/03	10				
	A	05/05	06/05	6	C	28/10	29/10	7	B	10/03	15/03	7				
	C	11/05	12/05	6	D	30/10	31/10	9	A	17/03	19/03	7				
	Total	18/04	12/05	41	Total	10/10	31/10	45	Total	24/02	19/03	39				

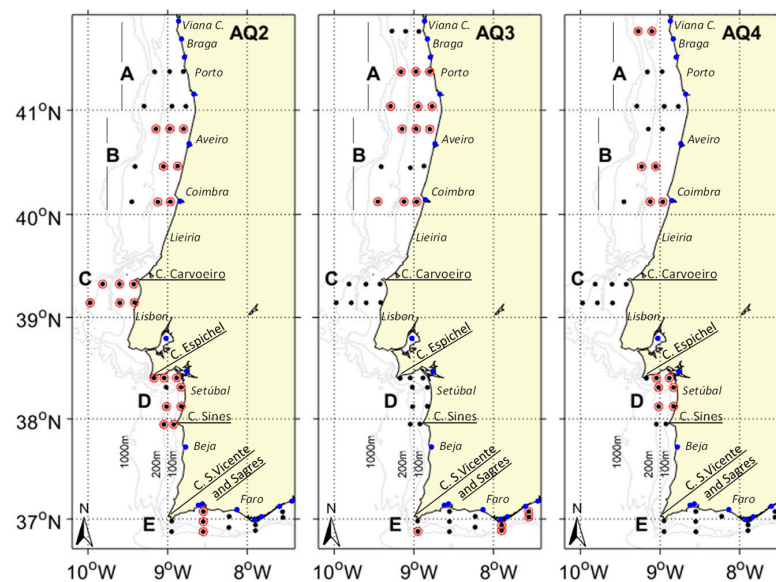


Figure 1. Location of in situ sampling stations (black dots, N = 125) and their matches with OC-CCI data (red circle, N = 53) in the five regions (A, B, C, D, and E). The AQ2 campaign was carried out in April/May 2019 (spring), AQ3 in October 2019 (autumn), and AQ4 in February/March 2020 (early spring). The main capes (Carvoeiro, Espichel, Sines, and São Vicente-Sagres; black lines) and the main points of freshwater entrance (from north to south: Minho, Lima, Ave, Douro, Ria de Aveiro, Mondego, Tagus, Sado, Mira, Odiáxere, Arade, Quarteira, Ria Formosa, Gilão, and Guadiana; blue dots) are identified on the map. Isobaths of 100, 200, and 1000 m (m) were obtained from GEBCO [25].

Surface seawater was sampled between ~4 and 6 m using Niskin bottles coupled to a rosette system and combined with a multiparametric probe (Ocean Seven 320 Plus WOCE-CTD, IDRONAUT, Brughiero, Italy) equipped with temperature ($^{\circ}\text{C}$), pressure (dbar), conductivity (mS cm^{-1}), and turbidity (FTU, SEAPOINT OEM) sensors (SEAPOINT, Exeter, NH, USA) (processing details are described in [26]). The dissolved inorganic nitrogen (DIN) was computed as the sum of NO_2^- , NO_3^- , and NH_4^+ (processing details are described in [22]). The seawater samples for chlorophyll *a* concentration (and phaeopigments) and light absorption coefficients analyses were kept refrigerated and in dark conditions until further processing, as described below.

2.2. Laboratory Work

2.2.1. Chlorophyll *a* and Pheopigments

A known volume ($\pm 1\text{--}3$ L) of seawater was filtered through 25 mm glass fibre filter GF/F ($0.7\ \mu\text{m}$ pore size). The filter was then placed in aluminium foil, stored in liquid nitrogen, and later transferred to a $-80\ ^{\circ}\text{C}$ ultra-freezer. The concentrations of chlorophyll *a* (Chl*a*, mg m^{-3}) and pheopigments (Pheo, the sum of pheophorbide *a* and pheophytin *a*, mg m^{-3}) were determined by High-Performance Liquid Chromatography (HPLC), using a Shimadzu Prominence-i LC-2030C 3D instrument (Shimadzu, Kyoto, Japan) with a C8 reversed phase column. Pigments were extracted with 3 mL of 95% cold buffered methanol (2% ammonium acetate) with $0.005\ \text{mg L}^{-1}$ of trans-beta-apo-8'-carotenal. The extracts were filtered (Fluoropore PTFE filter membranes (Merck KGaA, Darmstadt, Germany), nominal pore size $0.2\ \mu\text{m}$) into the flask with 0.4 mL of ultrapure water to avoid a distortion of their early elution peaks [27] and immediately injected into the HPLC [28–31]. Chl*a* was defined by the sum of allomers and epimers of divinyl chlorophyll *a*, chlorophyllide *a*, and chlorophyll *a* [32]. TChl*a* includes Chl*a* plus the sum of pheopigments (Pheo). The quality control of the pigment data was performed following the first rule described by [33].

2.2.2. Light Absorption Coefficients

Seawater samples were also analyzed to obtain the light absorption coefficients of coloured dissolved organic matter (CDOM, a_g) and particulate matter (a_p), which includes phytoplankton (a_{ph}) and inorganic particles (detritus, a_d).

For the absorption coefficient of the CDOM (a_g , m^{-1}), the seawater samples and a blank reference (used to subtract the water's absorption, using ultrapure water) were filtered through polycarbonate filters with a pore size of $0.2\ \mu\text{m}$ [34]. The residual water was stored in sterile amber glass bottles at $4\ ^{\circ}\text{C}$ until laboratory analysis [35]. The absorbance reading of the reference (blank) and samples (in triplicates) was performed using 100 mm acid-cleaned quartz cuvettes in a double-beam spectrophotometer (model Shimadzu 2600 series (Shimadzu, Kyoto, Japan)), from 300 to 800 nm [34]. The a_g (λ) (m^{-1}) was determined from the absorbance measurement multiplied by a conversion factor (natural logarithm, 2.303); divided by the cuvette length (m), with an offset correction at 650 nm; and subtracting the water absorption using the blank references of each measurement [34].

For the absorption coefficients of the particulate matter (a_p , m^{-1}), a known volume ($\pm 1\text{--}3$ L) of seawater was filtered through 25 mm glass fibre filter GF/F ($0.7\ \mu\text{m}$ pore size). The filter was placed in a vial, immediately frozen in liquid nitrogen, and stored in an $-80\ ^{\circ}\text{C}$ ultra-freezer. The spectral a_p , a_d , and a_{ph} (300–800 nm) were determined using the Transmittance %–Reflectance % (T-R) method described by [36,37], with a dual-beam spectrophotometer (Shimadzu model 2600 series) coupled to an integrating sphere. The a_d (λ) was measured after filter depigmentation with NaClO 1% [35]. The absorbance was converted to absorbance in suspension using the pathlength amplification factor of [38] for the T-R method. Finally, a_d (λ) was subtracted from a_p (λ) to obtain a_{ph} (λ). The phytoplankton-specific absorption coefficient (a_{ph}^* , $\text{m}^2\ \text{mg}^{-1}$) was obtained by normalizing a_{ph} by Chl*a* ($N = 122$). The sum of the biogenic absorption coefficients (a_{ph} , a_d and a_g) corresponded to a_{t-w} , and a_t to the total absorption coefficient including pure water (a_w) [39].

The spectral slope absorption (S) for a_g (S_g), a_d (S_d), and the sum of these components, namely a_{dg} (S_{dg}), was determined by fitting the absorption coefficients to a single-exponential non-linear curve ([40], $S(\lambda) = a_x (\lambda - \lambda_{\text{reference}}) \exp(-S [\lambda - \lambda_{\text{reference}}])$), between wavelengths from 350 nm to 500 nm, with 443 nm as the reference [41–43].

2.3. Satellite Data and Derived Products

The approach implemented in this study follows the diagram presented in Figure 2. $\text{Chl}a$ concentrations and bio-optical properties (absorption coefficients) were derived from OC-CCI reflectance data, as explained below.

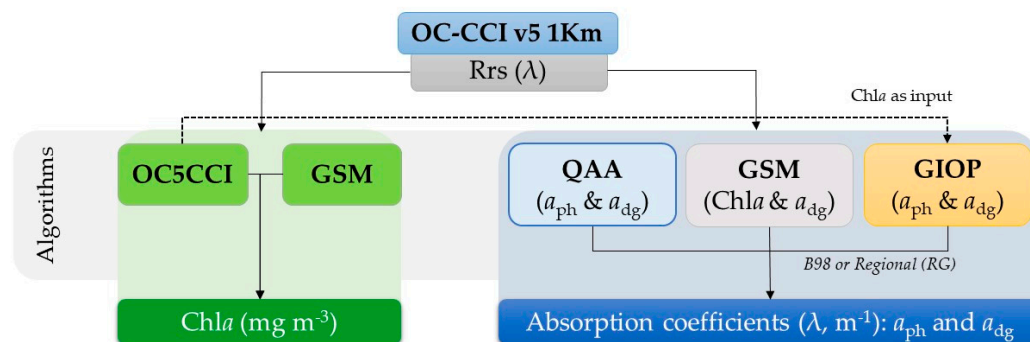


Figure 2. Schematic representation of the satellite data processing routine implemented to derive $\text{Chl}a$ concentrations and bio-optical properties (a_{ph} and a_{dg}).

2.3.1. Reflectance Data

Daily remote sensing reflectances (R_{rs} , sr^{-1} at 412, 443, 510, 560, and 665 nm) elaborated within the scope of the ESA Ocean Colour Climate Change Initiative project (OC-CCI, version 5, level 3 and 1 km spatial resolution) were obtained from the OC-CCI webserver (<https://www.oceancolour.org/>, accessed on 5 January 2022). This dataset integrates information from several sensors—SeaWiFS, MODIS, MERIS, VIIRS, and OLCI-3—using the unified processing chain described in [44].

2.3.2. Satellite-Derived Chlorophyll a

$\text{Chl}a$ concentrations were derived from OC-CCI v5, which uses the OC5CCI empirical algorithm for case 1 and case 2 waters [45], developed by IFREMER and PML. The OC5CCI algorithm (from CMEMS webserver <https://data.marine.copernicus.eu>, CMEMS-OC-QUID-009-034-036-046-047-066 to 069-087 to 092, accessed on 5 January 2022) was chosen based on a CMEMS calibration and sensitivity analysis, which evaluated several algorithms (OC3, OC4ME, OCI, OC5CI, OC5, OC5CCI). This analysis includes an in situ database of 191 samples from the coastal waters of Portugal [46] and has demonstrated its superior performance, with R^2 values of 0.89 compared to, e.g., OC4Me 0.78, and outperformed the OC's algorithms using the database from the AQUIMAR project, considering its four oceanographic cruises. Additionally, the $\text{Chl}a$ concentrations, as one of the products derived from the default semi-analytical GSM algorithm (Garver–Siegel–Maritorea, [47]), presented below were obtained for comparison with the empirical results of the OC5CCI.

2.3.3. Satellite-Derived Absorption Coefficients

Absorption coefficients (a_t , a_{ph} and a_{dg}) were also derived from the R_{rs} of OC-CCI v5 using three semi-analytical approaches: (i) the QAA (Quasi-Analytical Algorithm, [48]) derived from OC-CCI v5; (ii) the default version of the GSM (Garver–Siegel–Maritorea, [47]) algorithm; and (iii) the default version of the GIOP (Generalized Inherent Optical Property) algorithm (from [49]). These approaches, based on radiative transfer equations, relate the spectral distribution of R_{rs} to the inherent optical properties of water. Such algorithms continue to be used in the provision of standard products by the main projects of space agencies (e.g., the ESA and NASA).

Both the GSM and GIOP approaches were parameterized with coefficients from [50] to ensure consistency. In addition, GIOP was also parameterized with regional coefficients (regional a_{ph}). New regional coefficients (named RG) for the relationship between in situ Chl a and absorption coefficients (a_{ph}) were derived for the coastal waters of Portugal (N = 122). This was implemented following the approach described by [50,51], using the power law function coefficients for the entire spectral range ($\lambda = 400$ to 700 nm). See Section 3.3 for details on this regional parameterization.

A relevant difference between the default GIOP and the other approaches is that GIOP needs Chl a as an input component. In this case, OC5CCI Chl a was used, given the best performance of the algorithm (as presented in Section 3.4). Thus, the GIOP approach was also implemented using two variants: (i) GIOP using OC5CCI-derived Chl a as its input, with coefficients from [50] (GIOP-OC5CCI); and (ii) GIOP using OC5CCI-derived Chl a as its input and parameterized with regional coefficients (regional a_{ph} , GIOP-OC5CCI-RG). In total, 4 different results for satellite-derived absorption coefficients were obtained; three using standard approaches and one using regional coefficients.

2.3.4. Matchup Analysis

The dataset was processed according to the provided quality index, leaving a total of 53 matchups (Figure 1, red circles). As the data acquisition of the sensors (SeaWiFS, MODIS, MERIS, VIIRS and OLCI-3A) used in the OC-CCI product vary between $\sim 10:00$ and $\sim 13:30$ local solar time, the acceptable time window was initially set to ± 6 h (following [52]), however, subsequent tests showed a minimal significant effect in accepting in situ samples (N = 7) at any time of the same day. Hence, the time window was set to the same day [9]. To ensure spatial homogeneity, the median of a 3×3 window box centred on the sampling site was obtained based on Rrs (sr^{-1} , between bands 412 and 665 nm), with at least 5 valid pixels, a coefficient of variation less than 0.20, and pixels that differ by less than one standard deviation [9,53]. A comparative analysis of the Rrs between OC-CCI and Sentinel-3A (OLCI, N = 22) demonstrated a consistent pattern, with a slope exceeding 0.91 and a coefficient of determination (R^2) of 0.65 at 442 nm, 0.85 at 665–670 nm, and over 0.93 for other wavelengths (unpublished data). The 1 km spatial resolution dataset from OC-CCI, utilizing 3×3 window values without pixel overlap, could yield more matches and offer valuable insights into variability [44]. Despite Sentinel 3-A's higher resolution (300 m), OC-CCI's broader temporal coverage is advantageous for future comprehensive seasonal analyses.

To assess the agreement between in situ observations and the OC-CCI satellite's ocean colour products, a Type-2 regression least squares fit was applied (lsqfitma.m routine from MBARI, <http://www3.mbari.org>, accessed on 10 January 2022). Concomitant results (or matchups) were evaluated using regression parameters (coefficient of determination— R^2 —and linear equation parameters are provided in Supplementary Materials) and error estimations, including the bias (BIAS), mean squared error (RMSE), and mean absolute error (MAE). The BIAS and MAE were applied following [54].

Inherent optical properties (absorption coefficients) were aggregated within ± 3 nm of the OC-CCI bands. The 443 nm wavelength was chosen to represent the main variability of the biogenic absorption coefficients and is omitted hereinafter. Moreover, the a_t (443 nm) was evaluated to minimize the additional uncertainty introduced by partitioning a_t (443 nm) into its a_w , a_{ph} , and a_{dg} contributions [55].

2.4. Statistics and Data Analysis

The Shapiro–Wilk test was used to confirm the non-normality of the bio-optical parameters, and a Tukey honest significant difference (HSD) was performed to verify if there were mean significant differences between areas and campaigns (p -value < 0.05). Heatmaps of Kendall correlation coefficients (τ , ± 0 to 1, pairwise method) and their significance (** , p -value ≤ 0.05) were created using normalized in situ data. In addition, regression analyses were used to describe the relationships between in situ biogeochemical components (e.g.,

turbidity, Chl a concentrations) and absorption coefficients (a_t , a_{ph} , and a_{dg}). In order to obtain regional coefficients for the semi-analytical approaches, power law functions were fitted to the data, following [50] and [56]. These relations are presented with their R^2 , number of samples (N), and the coefficients (“a” and “b”) from a power law fit ($a \cdot x^b$) or polynomial fit (“Poly fit”, $a \cdot x + b$, when specified).

3. Results

3.1. Case 1 vs. Case 2 Waters

The total non-water absorption coefficient a_{t-w} varied between 0.05 and 0.44 m^{-1} (Table S1; Figures 3 and S1), reaching higher values ($>0.22 m^{-1}$) during the spring (AQ2) and early spring (AQ4) campaigns. During the spring campaign (AQ2), a_{t-w} (average 0.16 m^{-1}) demonstrated strong positive correlations ($\tau \geq 0.6$ *, Figure S2) with the phytoplankton components (Chl a , Pheo, and a_{ph} , e.g., in areas A and E), detritus absorption (a_d), and turbidity. CDOM absorption (a_g), became more strongly correlated to a_{t-w} in the autumn campaign (AQ3, average 0.12 m^{-1}), while during the early spring (AQ4, average 0.11 m^{-1}), the detritus and phytoplankton absorption coefficients became again more strongly correlated with a_{t-w} (Figure S2, except area D), but were not correlated with each other in the northern areas. The early spring campaign, which occurred during the initial phase of a strong upwelling event [22], was characterized by the highest turbidity (on average up to 1.19 FTU), DIN (up to 2.17 $\mu mol L^{-1}$ for areas A, B, and C), and a_d (average 0.020 m^{-1}), especially in the northern–central WIC (Figures 4 and S1; Table S1).

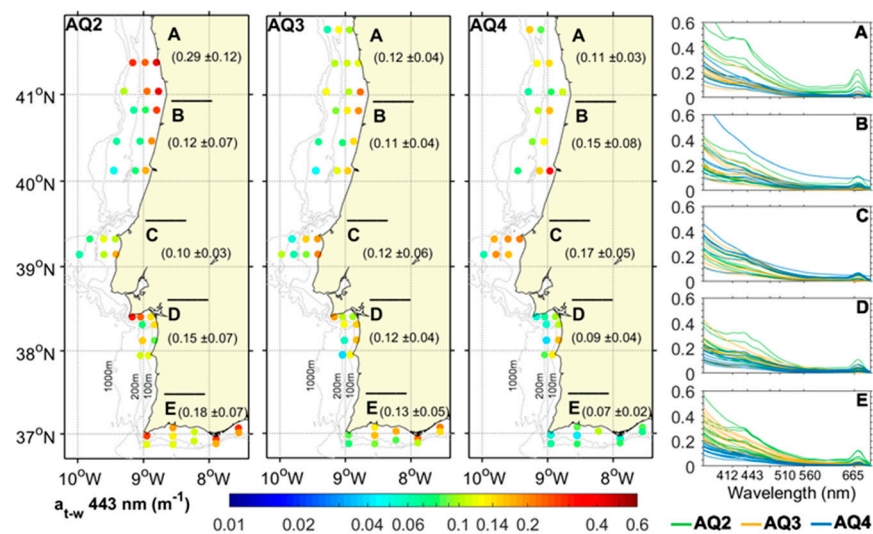


Figure 3. Distribution map of the total in situ absorption coefficients ($a_{t-w} m^{-1}$, without the sum of water absorption, $N = 125$) at wavelength (λ) 443 nm and their respective spectra ($\lambda = 350$ to 700 nm) by area (A to E) and oceanographic campaign (AQ2—spring, AQ3—autumn, and AQ4—early spring).

Following the [57] classification scheme, Case 1 waters (Figures 4 and S3), dominated by a_{ph} ($>70\%$ of a_{t-w}), represented only 23.2% of the samples and were most frequent in spring (during a phytoplankton bloom) (e.g., AQ2, area A and E) and early spring (AQ4, areas B and D) and had the lowest a_g contribution. Case 2 waters (Figure 4) were much more frequent, representing 76.8% of the samples within the WIC; of that, 64% were dominated by $a_{ph} + a_g$, 8% by a_g , 2.4% by $a_{ph} + a_d$, and 2.4% by all three biogenic absorption components. In approximately 58% of the samples, a_{ph} contributed between 50 and 70% of the biogenic absorption, mostly during the spring (AQ2) and early spring (AQ4) campaigns. A greater dominance of the CDOM component (38% of samples) was mainly observed during the autumn campaign (AQ3, e.g., area E). The detritus component had a higher contribution ($>50\%$) during the early spring campaign (AQ4), especially in the northern–central WIC (areas B and C).

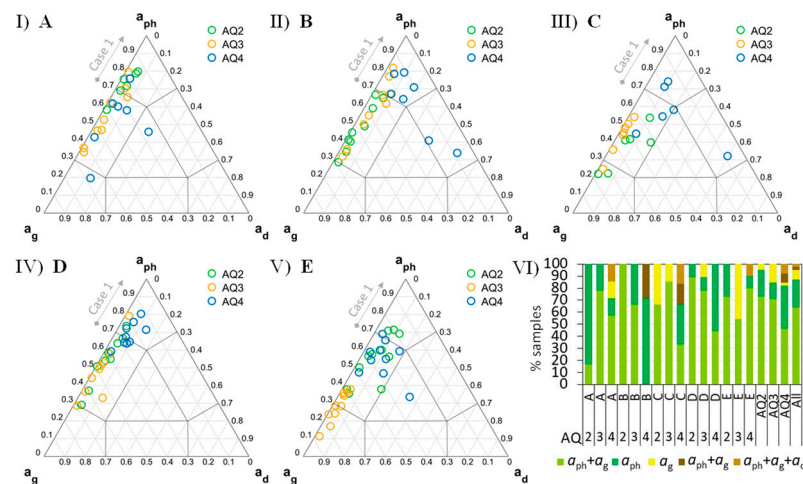


Figure 4. Triangular diagram (I to V) representing the contribution of the in situ absorption coefficients of phytoplankton (a_{ph} at 443 nm, m^{-1}), non-algal particles (NAPs, at 443 nm, m^{-1}), and coloured dissolved organic matter (CDOM, a_g at 443 nm, m^{-1}) by sampled area (A to E) and oceanographic campaign (AQ2—spring, AQ3—autumn, and AQ4—early spring). The bar graph (VI) shows the percentage (%) number of samples by area and campaign for each type of water [57], named according to the contribution of their components: $a_{ph} + a_g$, a_{ph} , a_g , $a_{ph} + a_d$, and $a_{ph} + a_g + a_d$.

3.2. Temporal and Spatial Variation of Bio-Optical Properties

The phytoplankton absorption coefficient (a_{ph} 443 nm, Figure 5), phytoplankton-specific absorption (a_{ph}^* 443 nm, Figure S4), and Chl a ranged from 0.01 to 0.35 m^{-1} , 0.03 to 0.017 $m^2 mg^{-1}$, and 0.10 to 9.38 $mg m^{-3}$, respectively (Table S1 and Figure S1), within all campaigns. The spring campaign (AQ2), sampled during a weakening upwelling event, was significantly different (p -value < 0.05) from the other campaigns regarding the a_{ph} and Chl a , associated with a phytoplankton bloom [22]. These differences in a_{ph} and Chl a were particularly pronounced in areas A, D (next to Cape Carvoeiro), and E, where the highest values were registered (>0.19 m^{-1} and >4 $mg m^{-3}$, respectively; Table S1, Figures 5 and S1), concurring with the lowest a_{ph}^* values (<0.04 $m^2 mg^{-1}$, e.g., area E, Figure S4). In this period (AQ2) and areas (A, D and E) characterized by enhanced productivity, Pheo values were also higher (>0.4 $mg m^{-3}$, Table S1), but still representing less than 30% of TChl a . In autumn (AQ3) and early spring (AQ4), the maximum of a_{ph} , a_{ph}^* , Chl a , and Pheo did not surpass 0.13 m^{-1} , 0.14 $m^2 mg^{-1}$, 3.34 $mg m^{-3}$, and 0.31 $mg m^{-3}$, respectively, excluding only one station in area E (AQ3), where Pheo registered 1.53 $mg m^{-3}$ (Table S1). This area in the southern WIC (E) had, in contrast, the lowest values of Chl a (<1.36 $mg m^{-3}$) and a_{ph} (<0.82 m^{-1}), which were associated with a higher sea surface temperature (AQ3) or higher salinity (AQ4) (Figures S2 and S5I,II). The proportion of Pheo in relation to Chl a was greater than ~30% in a few sample stations ($N = 6$), especially in autumn (Figure S5IV, e.g., AQ3 area E), however, no significant differences were observed between Chl a and TChl a when considering all sampling data ($N = 122$).

The detritus' absorption (a_d , m^{-1}) varied between 0.0004 and 0.194 m^{-1} (Table 1; Figures 5 and S1). The a_d was higher near the coastline, displaying a positive correlation (Figure S2) with several parameters related to the OACs during the spring (AQ2) and autumn (AQ3) campaigns. However, during the early spring (AQ4), a_d was significantly different, with high values (0.194 and 0.124 m^{-1}) in areas B and C. During this campaign in particular (AQ4), the correlation between a_d and turbidity became stronger. On the other hand, a reduction in the correlation power between a_d and phytoplankton was observed, except for in area D.

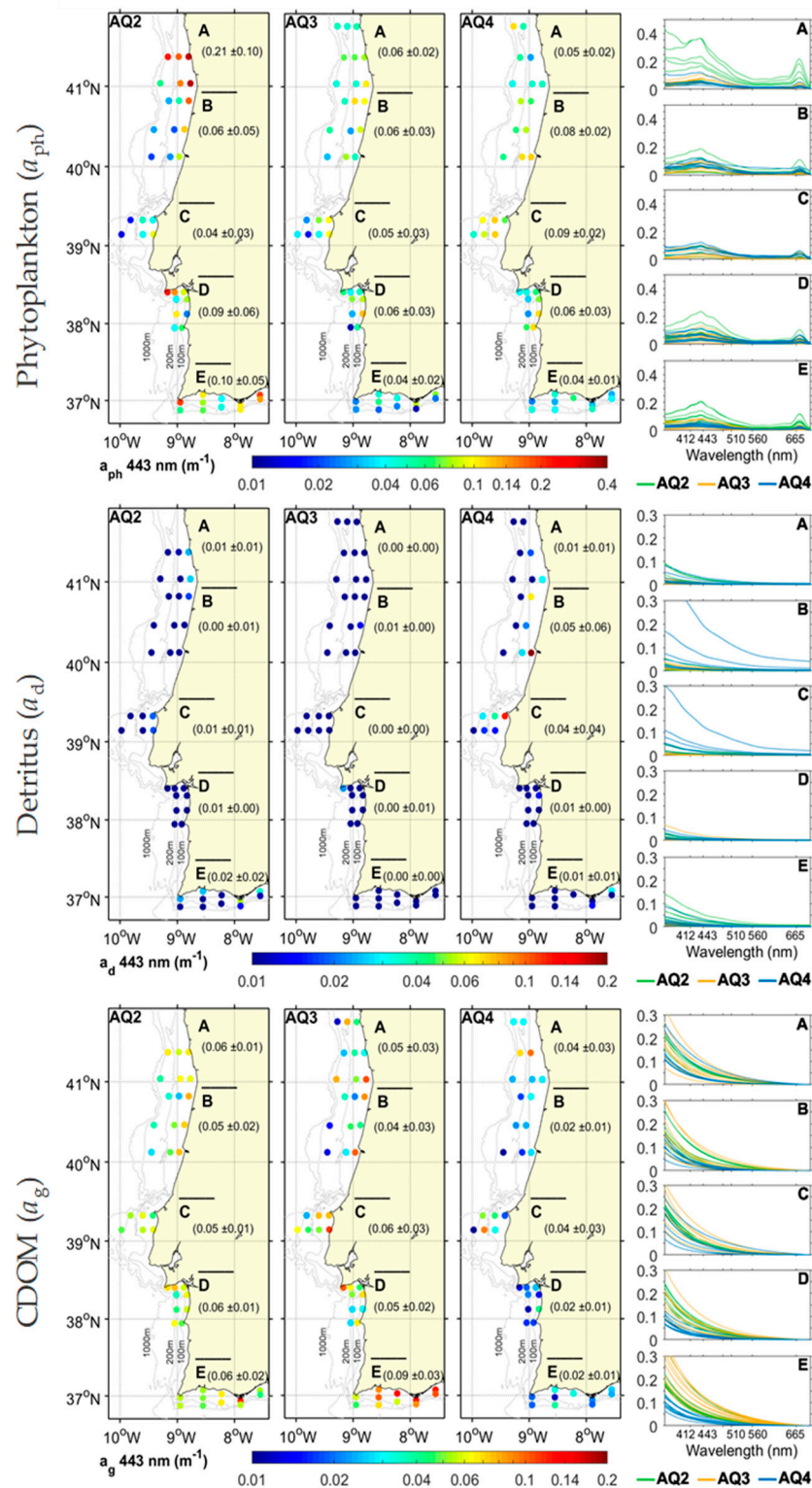


Figure 5. Spatial variation of phytoplankton absorption coefficient (a_{ph} , m^{-1}), non-algal particles or detritus (a_d , m^{-1}), and CDOM (a_g , m^{-1}), at wavelength (λ) 443 nm and their respective spectra ($\lambda = 350$ to 700 nm) by area (A to E) and oceanographic campaign (AQ2—spring, AQ3—autumn, and AQ4—early spring).

The absorption coefficient of the CDOM (a_g , m^{-1} , Table 1; Figures 5 and S1) ranged from 0.008 to 0.127 m^{-1} . The average values of a_g were similar between the spring (AQ2) and autumn (AQ3) campaigns, with a higher a_g (>0.09 m^{-1}) in area E, especially during

autumn. The a_g (Figure 5) sampled during the strong upwelling in early spring (AQ4), was significantly different from the other campaigns, which showed a much lower a_g ($<0.04 \text{ m}^{-1}$), especially in areas B, D, and E. This contrasts with the highest turbidity and DIN values also recorded in this campaign (AQ4) (northern areas) and the lowest salinities in area B, near the Mondego estuary (Figure S1 and Table S1).

3.3. Relationships between Biogeochemical Components and Bio-Optical Properties

The a_{ph} coefficients tended to increase (and the a^*_{ph} coefficients tended to decrease, Figure S5V–VIII) with increasing Chla (or TChla) in a power law function. For wavelengths from $\lambda = 400$ to 700 nm , new regional coefficients (named RG) were calculated using the relationship between in situ Chla and $a_{ph}(\lambda)$ for the coastal waters of Portugal ($N = 122$). As an example, Figure 6 presents the relationship between Chla and a_{ph} for the specific wavelength of 443 nm . The relationship obtained herein was closer to that reported in B04 [58] and L10 [56] than in B98 [50] and B10 [42] (Figures 6 and S6). This could be related to an overestimation of the Chla by the fluorimetric measurements included in the B98 and [51] global fits, as discussed by [42]. Inverting the relation, the a_{ph} (443 nm) vs. Chla derived from our dataset (Figure 6II, Table S2) was closer to the relation used in the Algal 2 (A2) algorithm for the North Sea [59,60] than the regional relation obtained by S15 [52] for the WIC. Both relations, that between Chla vs. a_{ph} (443 nm) and vice versa (Table S2), show a better agreement in the spring (AQ2) and autumn campaigns (AQ3) compared to the early spring campaign (AQ4). The highest errors were, in general, related to stations with a higher a^*_{ph} (e.g., area D in AQ2) and a higher proportion of Pheo in relation to Chla ($>30\%$).

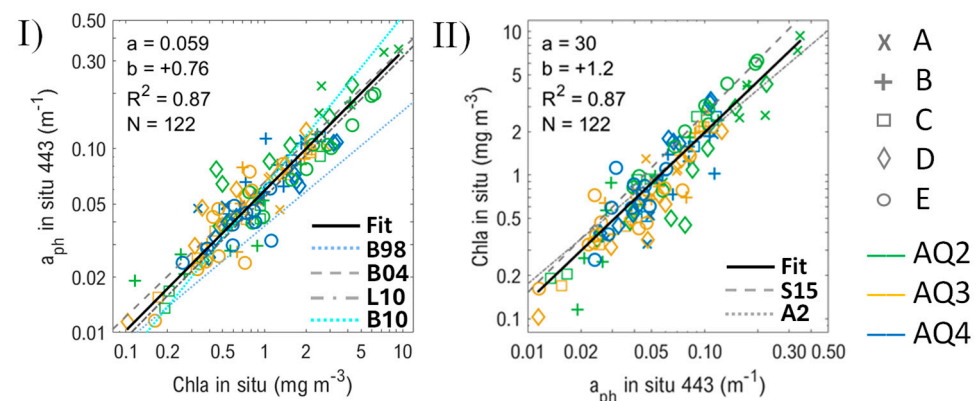


Figure 6. (I) Relationships between the in situ Chla (mg m^{-3}) and phytoplankton absorption coefficient (a_{ph} at 443 nm , m^{-1}) obtained by fitting a power law function (“Fit”, with coefficients “a” and “b”, r-squared: R^2 , and the number of samples: N). The relationship between Chla and a_{ph} was compared to the results obtained by Bricaud et al. [42,50,58] (B98, B04, and B10, respectively) and Loisel et al. [56] (L10). (II) a_{ph} versus Chla, which was compared to the results obtained by Sá et al. [52] (S15) and the Algal 2 (A2) algorithm [60]. The symbols correspond to different sampled areas (A to E), with different colours representing each oceanographic campaign (AQ2—spring, AQ3—autumn, and AQ4—early spring).

Despite the slightly stronger correlation between a_d and Chla during spring (AQ2) ($R^2 = 0.42$, Table S3), most samples were scattered and, in general, positioned below the fit obtained by B10 for oceanic waters (Figure 7I and Table S3, except some samples in AQ4). The relationship between a_d and turbidity (FTU) was described through a power law equation (Figure 7II) which showed a high covariation ($R^2 = 0.92$), with higher deviations related to lower a_d values, especially in the autumn (AQ3) campaign (Table S3). Figure S7 shows a negative relationship between a_d and temperature, as well as a more scattered pattern with salinity. The spectral slope S_d (nm^{-1}) had a relatively strong negative relation with a_d (Figure 7IV), with higher deviations in some stations with lower a_d ($<0.005 \text{ m}^{-1}$).

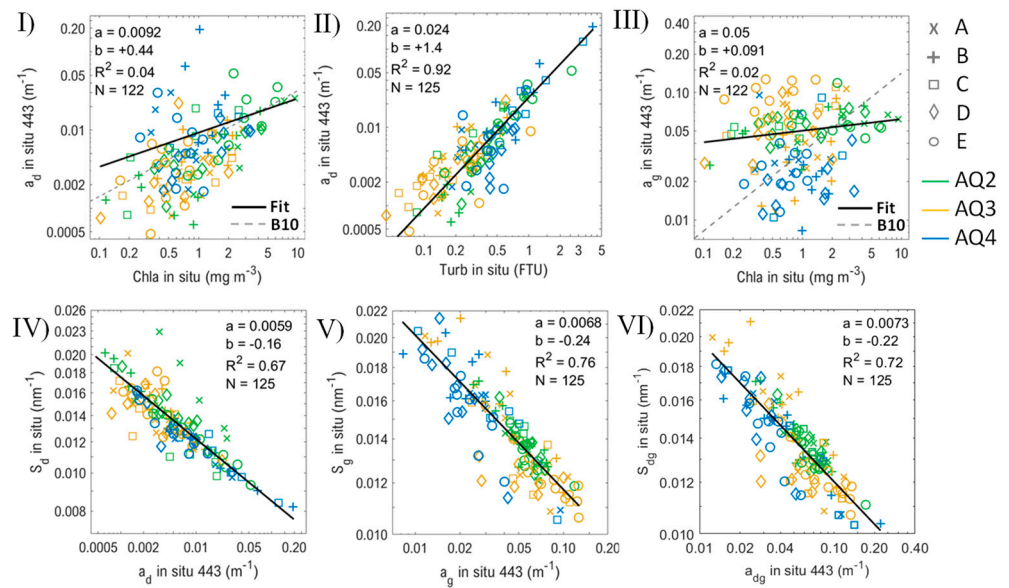


Figure 7. Relationships between (I) in situ absorption coefficient of non-algal particles (a_d , m^{-1}) and in situ Chla ($mg\ m^{-3}$); (II) in situ absorption coefficient of non-algal particles (a_d , m^{-1}) and turbidity (Turb, FTU); (III) in situ absorption coefficient of coloured dissolved organic matter or gelbstoff (a_g , m^{-1}) and in situ Chla ($mg\ m^{-3}$); (IV) spectral slope of detritus (S_d , nm^{-1}) and the absorption coefficient of non-algal particles (a_d , m^{-1}); (V) spectral slope of CDOM (S_g , nm^{-1}) and the absorption coefficient of CDOM (a_g , m^{-1}); and (VI) spectral slope of detritus + CDOM (S_{dg} , nm^{-1}) and the absorption coefficient of detritus + CDOM (a_{dg} , m^{-1}). The fit curve was obtained by a power law function (“Fit”, with coefficients “a” and “b”, r-squared: R^2 , and number of samples: N). Comparisons with the curves obtained by B10 [42] are also presented. The symbols correspond to different sampled areas (A to E), with different colours representing each oceanographic campaign (AQ2—spring, AQ3—autumn, and AQ4—early spring).

In general, CDOM’s relationships with the other parameters were very scattered (Figures 7 and S8; Table S4), suggesting great variability in its origin and state, which is confirmed by its weak ($\tau < 0.3$) and non-significant correlations with most parameters (Figure S2). Each campaign showed a different behaviour concerning a_g variability. The a_g was significantly correlated (Figure S2) with Chla, turbidity, and DC in spring (AQ2); with salinity, detritus, turbidity, Pheo, and DC in autumn (AQ3); and with only DIN in the early spring (AQ4). The S_g (nm^{-1}) and S_{dg} (nm^{-1}) had a strong negative relation with a_g and a_{dg} , respectively (Figure 7V,VI).

3.4. Evaluation of Semi-Analytical Approaches to Deriving Bio-Optical Properties from Ocean Colour

The Chla retrievals with OC5CCI and GSM algorithms were evaluated to determine the optimal input for the GIOP algorithm. In this study, the Chla retrieved with the empirical OC5CCI algorithm (Figure 8I, $N = 53$) yielded good statistical results ($R^2 = 0.77$) which were superior to those obtained by the standard GSM ($R^2 = 0.50$, Figure 8II), but still with some degree of underestimation for most cases (BIAS 0.87; Figure 8I). According to [54], a BIAS < 1.0 indicates underestimations.

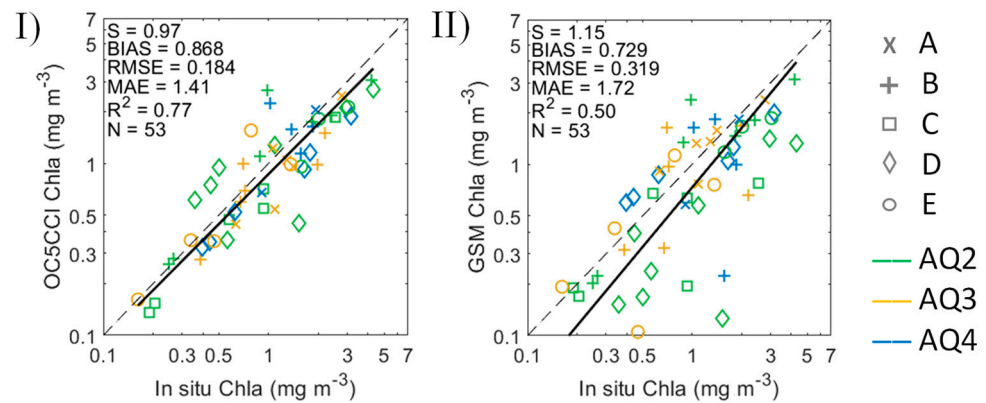


Figure 8. Comparison between in situ Chla (mg m⁻³) and its corresponding retrievals using the (I) OC5CCI algorithm (OC-CCI) [9] and (II) Garver–Siegel–Maritorena—the GSM algorithm [57]. The symbols correspond to different sampled areas (A to E), with different colours representing each oceanographic campaign (AQ2—spring, AQ3—autumn, and AQ4—early spring).

The comparison between the in situ absorption coefficients (a_t , a_{ph} , and a_{dg} , N = 53) and their corresponding retrievals obtained by the standard semi-analytical algorithms QAA, GSM, and GIOP (with Chla OC5CCI as input) are presented in Figure 9. All standard semi-analytical algorithms underestimated the total absorption retrievals (a_t , BIAS ~ 0.69 to 0.75) and exhibited a mean absolute error (MAE) ranging from 1.45 to 1.53 (Figure 9I,IV,VII; Table S5).

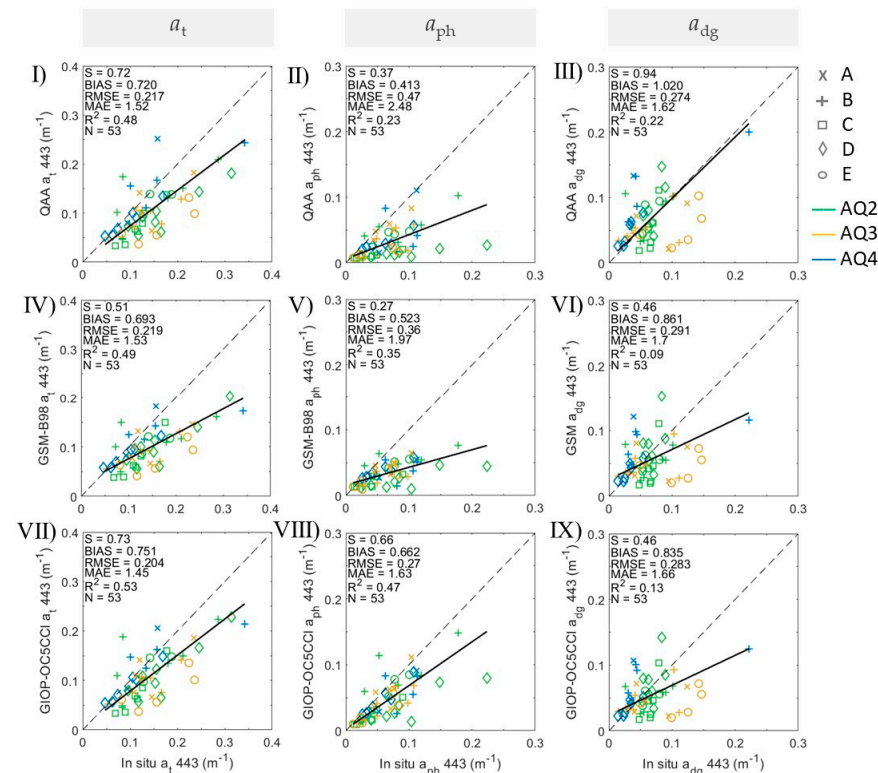


Figure 9. Comparison between in situ absorption coefficients (a_t , a_{ph} , and a_{dg} at 443 nm, m⁻¹) and their corresponding retrievals, obtained by default algorithms—the QAA from OC-CCI v5 (I)–(III)), GSM (IV)–(VI)), and GIOP—using Chla OC5CCI retrievals as their input (GIOP-OC5CCI; VII)–(IX)). The symbols correspond to different sampled areas (A to E), with different colours representing each oceanographic campaign (AQ2—spring, AQ3—autumn, and AQ4—early spring).

The a_{ph} retrievals were even more underestimated (BIAS 0.41 to 0.66), especially for three cases in spring with highly underestimated values (AQ2, Figure 9II,V,VIII, green diamond—area D;

Table S5). The GIOP algorithm, utilizing Chl a retrievals from OC5CCI as its input, achieved the smallest underestimation in a_{ph} retrievals, yielding the best statistical outcomes (MAE = 1.63, $R^2 = 0.47$, and $S = 0.66$). In contrast, the QAA and GSM's (using B98 coefficients) retrievals exhibited substantial underestimations, with BIAS values of 0.41 and 0.52, respectively.

For the a_{dg} retrievals, on the other hand, the QAA yielded better results ($R^2 = 0.22$ and slope of 0.94), especially due to its improved estimate of the highest a_{dg} value in early spring (AQ4, Figure 9III, blue cross—in area B, where only one station exhibited the highest a_d values; Table S5). For all algorithm retrievals, including that of the QAA, significant underestimations were observed in cases with a higher a_g contribution in autumn (AQ3, Figure 9III,VI,IX, the yellow ones mostly in area E). The a_{dg} statistical results for the GSM and GIOP algorithms (MAE = 1.7 and 1.66, BIAS = 0.86 and 0.83, $R^2 = 0.09$ and 0.13, and both $S = 0.46$) were not significantly different.

Considering the results obtained with the standard GIOP algorithm for a_t and a_{ph} , the subsequent phase involved the use of the regional parameterization (RG) obtained for the power law relation between the in situ Chl a and a_{ph} (λ) instead of the B98 coefficients for the a_{ph} estimation [49] (Figure S6).

As expected, the results obtained with the regional coefficients (GIOP-OC5CCI-RG, Figure 10) were better than the standard GIOP version in terms of the a_t and a_{ph} coefficients. This was mainly related to a significant improvement in the a_{ph} retrievals, which consequently led to an improvement mostly in the slope results for a_t (0.78). The a_{dg} retrievals from the GIOP's regional version (Figure 10) were close to its standard results (Figure 9). The stations with the highest biases (3 for a_{ph} and 7 for a_{dg}) remained with high underestimations, even for the GIOP-RG.

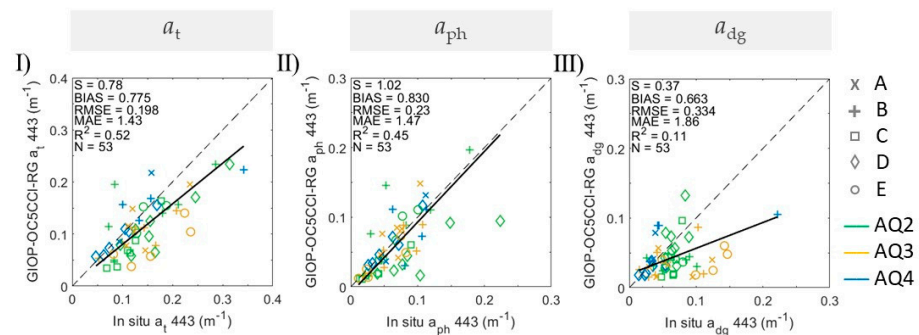


Figure 10. Comparison between in situ absorption coefficients (a_t , a_{ph} , and a_{dg} at 443 nm, m^{-1}) (I–III) and the GIOP, with Chl a OC5CCI retrievals as the input and using the RG coefficients (regional, Figure S5), namely the GIOP-OC5CCI-RG. The symbols correspond to different sampled areas (A to E), with different colours representing each oceanographic campaign (AQ2—spring, AQ3—autumn, and AQ4—early spring).

4. Discussion

4.1. Case 1 vs. Case 2 Waters

The Western Iberian Coast (WIC), located in an Eastern Boundary Upwelling System (EBUS), is characterized by dynamic coastal upwelling, with interactions between oceanographic features (e.g., capes and canyons) and continental river runoff. The interaction of the oceanic water masses with freshwater inputs governs the spatial distributions of the temperature, salinity, and nutrients, which in turn influence the optical properties of the surface waters. In the WIC, salinity shows a clear north–south gradient, with the lowest values (<35) in the northern region (e.g., areas A, B, and C) more influenced by continental runoff compared to the southern region (this study, [19,26,61]). Sea surface salinity, temperature, and the distance from the coastlines had weak but significant correlations (<0.4) with the OACs, denoting the high variability in the OACs' distribution at each coastal site and between different seasons.

The spring (AQ2) and early spring (AQ4) campaigns occurred during coastal upwelling events, but at different stages; the first at the end of this event, with a phytoplankton bloom on course, and the second in the initial phase, with a lower phytoplankton biomass but high nutrients [22], and a significant increase in turbidity and detritus, especially in the northern region of the WIC. Both the spring and early spring campaigns thus had the highest a_{t-w} values recorded, but with different contributions from OACs. For the spring campaign, a_{ph} (and Chl a) had a high correlation with a_d , denoting the main autochthonous source of the detritus, which was tightly linked to the phytoplankton bloom. The early spring campaign, on the other hand, had a lower a_{ph} contribution and higher a_d contribution to a_{t-w} , which covariates with turbidity but was not significant with Chl a . Hence, the non-algal particles in this case were not only regulated by the phytoplankton community (its growth and decay) but also associated with external sources linked to other coastal processes, such as seasonal sedimentary dynamics. This is similar to the observations made by [62] for coastal waters in the Eastern English Channel. Higher coastal water turbidity in the WIC was also observed by [63] in the winter and early spring months, associated with more intense wave action, resuspending bottom sediments, especially across the wider northern shelf (during winter) added to initiating coastal upwelling events in the early spring, as sampled during AQ4. Moreover, [64] has previously reported the importance of internal waves in the resuspension of sediments and bottom currents near the Nazaré Canyon (next to area C). Winter is also the rainy season in Portugal [19], and river runoff was also likely a source of the higher a_d and turbidity values observed, especially at the coastal stations nearest to Porto city (area A), the Mondego River (area B), and Cape Carvoeiro (area C), during the following early spring season (AQ4). In fact, [65] identified seasonal variations in water type classification using satellite imagery. During winter and spring, the waters of the WIC were predominantly classified as Case 2 waters (complex waters), which exhibited higher CDOM per Chl a ratios compared to typical Case 1 waters. Case 1 waters were primarily observed in the southern and offshore regions during the autumn and summer seasons. In our case, due to the phytoplankton bloom, most Case 1 waters were found in the spring campaign. Sá [65] attributed the higher CDOM in Case 2 waters to biogenic material resulting from the degradation of phytoplankton blooms in spring and from riverine inputs in winter.

The autumn campaign had lower surface water turbidity, but similar a_{t-w} values compared to the early spring, in most stations. In this case, CDOM together with phytoplankton were the dominant optical constituents contributing to a_{t-w} . CDOM, however, had no correlation with Chl a , especially during the autumn and early spring campaigns. Only the spring campaign showed some correlation between CDOM and Chl a (0.3), which coincided with a phytoplankton bloom. Sá [65] reported a higher dominance of CDOM during the spring season in the Nazaré Canyon area, though the mean phytoplankton absorption value was lower than that observed in our study for the same period (0.033 m^{-1} and 0.098 m^{-1} , respectively). In our case, we also found a higher CDOM contribution in the southern WIC (area E), which is characterized by a lower contribution of river runoff and a narrower shelf [19]. Besides the contribution of continental runoff to the coastal waters of the WIC, another possible source that may explain the higher CDOM absorption and its relative contribution to a_{t-w} during the autumn campaign may be the degradation products released during the decay of phytoplankton blooms associated with coastal upwelling events. Hence, even if they are produced by autochthonous sources, the possible lag between phytoplankton growth and CDOM production, especially during and post-bloom decay phase, could maybe explain the temporal disconnection between CDOM and Chl a in highly dynamic coastal areas such as the WIC. In fact, the stations with the highest CDOM absorption contributions had also higher contributions of Chl a degradation products, i.e., Pheo. Less CDOM photobleaching processes, associated with the lower incident solar irradiance during the autumn months, may also partly contribute to the higher CDOM contribution in this season. Unfortunately, in this study, it was not possible to further investigate the possible sources of CDOM due to limited spectral a_g information

and auxiliary data. Further studies using more spectrally resolved a_g (220–700 nm) [66] and carbon pool measurements are encouraged to verify the sources of CDOM in the WIC, as well as their spatial and temporal variability.

Following [57]’s optical classification scheme, the majority (74%) of the samples collected during this study in the coastal waters of Portugal were classified as Case 2 waters (Case 1 corresponded to 23.2%), and most of the samples were dominated by $a_{ph} + a_g$. The autumn and early spring seasons, under non-bloom conditions, are especially characterized by more complex Case 2 optical water types, with higher detritus and CDOM contributions to the a_{t-w} . The present results are consistent with the findings obtained by [65] for similar areas of the Portuguese coast and those of [67] in the Sagres region (the west area, E), which identified a majority of a_{ph} optically dominated waters, but also with an important contribution of a_g , varying between 33 and 60% of a_{t-w} during bloom and non-bloom conditions, respectively.

4.2. Temporal and Spatial Variation of Bio-Optical Properties

As discussed in the previous section, the WIC presents high temporal and spatial bio-optical variability, regulated by highly dynamic coastal processes and some regional site-specific characteristics. Chl a and a_{ph} had high spatial variability, especially during the spring campaign (AQ2), which occurred during the end of a strong upwelling event [22]. Phytoplankton blooms (e.g., Chl a > ~5 mg m $^{-3}$, see [22]), dominated by microphytoplankton groups (diatoms and dinoflagellates, [68]), in response to coastal upwelling events (e.g., AQ2) are a common feature in the spring and summer months (April to September), along the west coast of Portugal, especially in the northern region [19,67–71], as well as around the Carvoeiro and Sagres capes (areas D and E, respectively), as shown in the present study. The a_{ph}^* spectra were mostly flattened during the spring and had lower values, especially at the stations with the highest Chl a (areas A and E). These areas also had high concentrations of fucoxanthin and peridinin (unpublished data), suggesting the dominance of phytoplankton groups with larger cells (e.g., diatoms and dinoflagellates), with a higher packaging effect [72]. The overall power law relation between a_{ph} (443) and Chl a , and the negative relation between a_{ph}^* (443) and Chl a , denotes the effects of intracellular pigment self-shading and the increase in accessory pigments observed in other studies [58].

Moita [69] examined the temporal and spatial variations of phytoplankton assemblages in the WIC and observed that phytoplankton’s biomass and diversity varied seasonally and spatially in response to the dominant oceanographic processes, with diatoms being the dominant group during spring and early summer, when northerly winds and upwelling conditions were prevalent, followed by dinoflagellates during late summer and autumn, when more stratified conditions in the water column developed. The study reported high concentrations of Chl a during the upwelling season in the WIC, with Chl a concentrations reaching up to 6 mg m $^{-3}$. Goela et al. [67] also investigated the contribution of phytoplankton to the optical properties of the southwest coast of Portugal and found that the a_{ph}^* varied according to the taxonomic composition of the phytoplankton assemblages, with diatoms having a lower a_{ph}^* than other phytoplankton groups. The authors also reported a negative correlation between a_{ph}^* and Chl a , with the highest values of Chl a seen during the upwelling season in the WIC, as observed in this study.

Brito et al. [17], on the other hand, reported a high specific absorption coefficient (an a_{ph}^* up to 0.17 m 2 mg $^{-1}$) associated with pico/nanophytoplankton cells during the summer months (August–September) in the western and southern coastal waters of Portugal (e.g., areas B, D, and E). A high a_{ph}^* (up to 0.17 m 2 mg $^{-1}$) was also observed in the present study in some offshore stations during the spring campaign (AQ2, at areas B and D), which may indicate a low packing effect associated with the dominance of smaller picophytoplankton cells [42]. This is supported by the higher presence of photoprotective pigments such as alloxanthin and zeaxanthin in these areas (unpublished data), suggesting the presence of cryptophytes (offshore of area D) and cyanobacteria (offshore of area B). In general, the a_{ph}^* values obtained in our study (except the highest values in areas B and D in AQ2) are close to the range of coefficients reported by [16] (0.02 to 0.12 m 2 mg $^{-1}$ at 440 nm) for the

Sagres cape (area E). Further analysis of a_{ph}^* variability and phytoplankton composition will be part of future work.

The early spring season was characterized by lower phytoplankton absorption and Chl a and higher detritus absorption, which was correlated to turbidity, suggesting the contribution of other sources rather than just phytoplankton degradation products, such as continental runoff, the bottom resuspension of sediments, and strong upwelling, as discussed in the previous section. CDOM absorption was higher in the autumn season along most of the inner shore stations within the WIC, which is probably attributed to post-bloom degradation products, in addition to continental runoff and resuspension, as previously discussed.

4.3. Relationships between Biogeochemical Components and Bio-Optical Properties

The relationship between a_{ph} (443 nm) and Chl a (and TChl a) obtained in the present study ($N = 122$) was similar to that found by [58] and [56] for global oceanic and coastal waters. Some minor deviations are likely attributed to local and regional phytoplankton species and ecophysiological conditions, with different proportions of photosynthetic and photoprotective pigments and packaging effects. The global relation proposed by Bricaud et al. [50,51] was somewhat offset, as also noticed by Bricaud et al. [42,58], who discussed the major differences as being related to the fluorimetric Chl a measurements which composed most of the previous global datasets, instead using only HPLC. This has important implications for ocean colour retrievals since standard default versions of the GIOP semi-analytical model are still presented with Bricaud et al.'s [50,51] global fit to derive the a_{ph}^* eigenvectors. Our results contrast with the findings obtained by [41] using a dataset from the Atlantic Ocean and the Mediterranean Sea, where a better agreement was obtained with [51]. In addition to the regional variability of the phytoplankton communities in coastal waters, regional departures from the average global parameterization are expected even for Case 1 waters, as discussed by [50,51], but they may occur more often in coastal waters [41].

The relationship between the a_{ph} (443 nm) and Chl a derived from our dataset was also close to the relation used in the Algal 2 algorithm derived from the MERMAID dataset (Meris Matchup in situ Database [60]). The regional relation found by [52,65] for the coastal waters of Portugal, sampled during the beginning of the spring season (30 March to 12 April 2011), was closer to the relation found in the autumn (AQ3) campaign in our study, probably due to the lower a_{ph} (443 nm, $<0.1\text{ m}^{-1}$) and Chl a ($<2\text{ mg m}^{-3}$) of both datasets. Higher deviations in the a_{ph} (443) and Chl a (and TChl a) relationships were observed for the early spring campaign (AQ4), likely due to changes in the phytoplankton assemblage [41,42].

The large variability observed around the a_g (443) versus Chl a relationships is a common feature [73,74]. Even in the open ocean, the part of the variance in a_g explained by algal biomass is generally rather low (e.g., [40,75]). CDOM exhibits significant variability due to biological processes (e.g., microbial and planktonic), photobleaching, inputs of CDOM, and nutrients from deep waters through vertical mixing, upwelling, or terrestrial sources. Regarding biological processes, this can also be attributed to the temporal decoupling between CDOM production and algal biomass growth [74], as previously discussed. Therefore, the CDOM's quantity may be reflecting the biological productivity of a previous bloom event, since CDOM tends to be a long-lived product of phytoplankton degradation. When the origin of CDOM is not local, for example, from the degradation of phytoplankton cells and other organic particles [76], it can be used as an indicator of the freshwater input into the system and riverine/estuarine discharge [77], as well as indicating sediment resuspension events in coastal waters. However, due to the non-significant (AQ2 and AQ4) or non-strong (AQ3) correlation between CDOM and salinity, this may not be the most of case for the WIC.

Regarding the relationship between a_d and Chl a , despite its scattered pattern, a better correlation ($R^2 = 0.42$) was achieved only during the period of higher phytoplankton biomass (AQ2), which closely resembled the relationship found by [42]. Nonetheless,

regardless of the sampled period, turbidity displayed a strong correlation with detritus, suggesting its potential utility for the satellite-based estimation of detritus from turbidity data for the coastal waters of Portugal.

4.4. Semi-Analytical Approaches to Deriving Bio-Optical Properties from Ocean Colour

The Chl a concentration estimated through the empirical OC5CCI algorithm [9] from OC-CCI data yielded better results than semi-analytical algorithms (GSM) for the WIC in the North Atlantic. The OC5CCI is an empirical approach adapted specifically to retrieving Chl a in coastal waters under the influence of suspended sediments from different sources [78], such as the WIC, and it proved to be a reasonable approach, at least for most cases. Sá et al. [52] also found that empirical algorithms adapted to coastal waters perform better than standard global approaches (e.g., OC4, [79]) within the WIC.

Nonetheless, the retrieval of a bulk set of IOPs using semi-analytical algorithms remains a challenge. The new regional coefficients (RG) from the in situ relation of Chl a and a_{ph} , used in the GIOP algorithm (GIOP-OC5CCI-RG) instead of the B98 coefficients, helped to improve the a_{ph} and a_t retrievals. Further improved results for phytoplankton absorption could be achieved using empirical relationships by directly applying the RG coefficients over Chl a OC5CCI (a_{ph} RG-OC5CCI, Figure 11), compared to the semi-analytical algorithms, due to the additional uncertainty introduced by partitioning a_t (443 nm) into its a_w , a_{ph} , and a_{dg} contributions [55]. Nevertheless, empirical algorithms still do not resolve complex cases, such as variations in the average a_{ph} vs. Chl a relation, with higher a_{ph}^* values seen for three stations in AQ2 (area D), which caused a_{ph} to have a higher underestimation for all approaches tested. Such variations may be linked to site-specific changes in the phytoplankton assemblage, as well as photoadaptation processes. Other factors that depart from average behaviours, such as one case in area B during spring (AQ2), which had a high overestimation, may be associated with higher turbidity, as empirical approaches tend to fail even with the OC5, which aims to determine the Chl a and suspended sediment in more complex coastal waters.

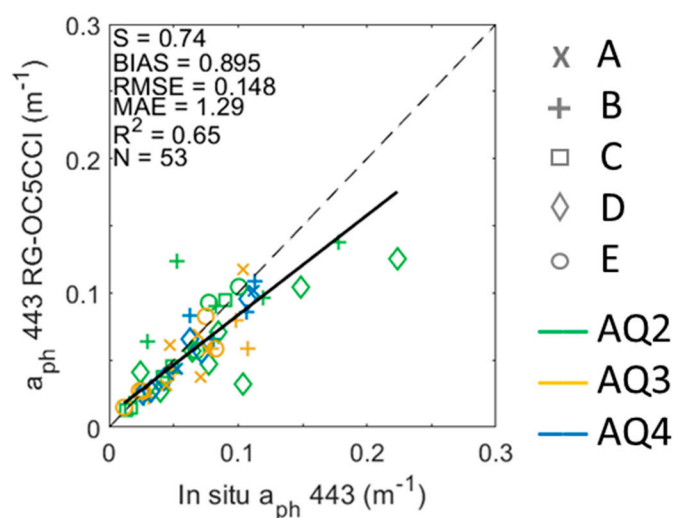


Figure 11. Comparison between in situ a_{ph} at 443 nm (m^{-1}) and the retrievals from the OC5CCI using the RG coefficients at 443 nm (Chl_a vs. a_{ph}). The dotted line is the 1:1 line, symbols correspond to different sampled areas (A to E), with different colours representing each oceanographic campaign (AQ2—spring, AQ3—autumn, and AQ4—early spring).

The QAA exhibited good results for higher a_d values, as expected in optically complex waters [80,81]. However, this algorithm, as well as the others tested, was not able to improve its estimates in the presence of high concentrations of CDOM. In the case of the GIOP, the default S_{dg} used to estimate the a_{dg} is a fixed value of $0.018 m^{-1}$, higher than the average $0.014 m^{-1}$ found in the present study. Nonetheless, recent works have shown that

the uncertainties in this algorithm have been more closely linked to the low performance in estimating the b_{bp} slope (η) [55]. Despite the fact that the GIOP algorithm uses the QAA method to estimate the b_{bp} spectral slope (band ratio R_{rs} 443 nm/ R_{rs} 560 nm, step 4, as described in [48]), a low correlation ($R^2 = 0.12$) between this band ratio and turbidity (commonly related to b_{bp} and η) was observed in this study. While GIOP and GSM are more suitable for Case 1 waters, they could eventually yield better results with regionalized parametrizations [82]. Considering the greater flexibility of the GIOP in applying different parameterization methods, it could be a strong candidate for regional parameterizations to improve algorithm performance in coastal environments. However, a robust database for coastal waters is still necessary to support these modifications [49,83].

Another source of uncertainty that was not analyzed in the present work due to the absence of in situ radiometric data, but which also affects the performance of bio-optical retrievals, is the accuracy of the satellite's CCI R_{rs} product. This product aggregates the R_{rs} from different sensors, including OLCI, VIIRS, and MODIS, for our study period, using the Polymer (v4.12) atmospheric correction. It is, however, known that atmospheric correction is challenging, especially in coastal environments, which have continental aerosols, optically complex waters, and continental adjacency effects. Several works have been dedicated to evaluating the accuracy of satellite R_{rs} products, including the CCI project [9], but this is an ongoing and continuous effort which needs to be included in future works within the WIC and elsewhere.

It is evident that the continuous adaptation and validation of these algorithms are necessary to ensure accuracy in coastal waters [49]. The development of regional parameterizations and the improvement of calibration and atmospheric correction procedures are fundamental steps to enhancing the accuracy of the inherent optical property (IOP) estimates for coastal waters provided by the QAA, GSM, and GIOP algorithms [84–88].

5. Conclusions

This study provided a comprehensive overview of the optical component variability in the WIC, representing an unprecedented investigation for this region, covering the entire coast and different seasons, including partitioned biogenic absorption coefficients and biogeochemical properties. Significant seasonal variability in bio-optical properties i.e., phytoplankton (Chl a), detritus, and CDOM absorption, was found due to factors associated with the changes in environmental conditions (e.g., upwelling and bottom resuspension) at each site. Furthermore, based on this robust in situ dataset, empirical relationships were established and are provided herein. This is a valuable contribution to the development of ocean colour algorithms. An overall validation was conducted using multi-sensor OC-CCI products for the estimation of absorption coefficients and Chl a in the WIC, involving a direct comparison between in situ reference measurements and retrievals from standard and regionally parametrized semi-analytical algorithms. A set of relevant outcomes and conclusions were obtained:

- A strong power law relation between turbidity and detritus suggests the potential for using satellite-based turbidity data to estimate detritus in coastal waters.
- In terms of the performance and limitations of algorithms, semi-analytical algorithms (QAA, GSM, GIOP) tended to underestimate the absorption coefficients, a common issue in coastal waters.
- The WIC regional coefficients (RG), derived from the relationship between in situ Chl a and a_{ph} , improved the results of the semi-analytical algorithm GIOP for a_{ph} (λ). Additionally, the RG coefficients improved the empirical results when applied directly to Chl a values obtained from the OC5CCI algorithm.
- These observations highlight the importance of regional-specific studies and the development of tailored algorithms to improve the accuracy of ocean colour remote sensing in diverse and dynamic coastal environments, especially for the analysis of the phytoplankton community's composition.

Supplementary Materials: The following supporting information can be downloaded at <https://www.mdpi.com/article/10.3390/rs16183440/s1>.

Author Contributions: Conceptualization, L.F., N.R. and A.C.B.; methodology, L.F., N.R. and A.C.B.; software, L.F.; validation, L.F.; formal analysis, L.F.; investigation, L.F.; resources, L.F., V.B., C.P. and A.C.B.; data curation, L.F. and A.T.; writing—original draft preparation, L.F., N.R. and A.C.B.; writing—review and editing, L.F., N.R., V.B., C.S., A.T., C.P. and A.C.B.; visualization, L.F., N.R. and A.C.B.; supervision, A.C.B., V.B. and N.R.; project administration, C.P. and A.C.B.; funding acquisition, C.P. and A.C.B. All authors have read and agreed to the published version of the manuscript.

Funding: This research was funded by the AQUIMAR-Marine knowledge supporting aquaculture Project through the Operational Programme MAR2020 (MAR-02.01.01-FEAMP-0107) and by the European Union’s Horizon 2020 Research and Innovation Programme under grant agreement N 810139: Project Portugal Twinning for Innovation and Excellence in Marine Science and Earth Observation—PORTWIMS. This work benefited from the Infrastructure CoastNet—Portuguese Coastal Monitoring Network (<http://geoportail.coastnet.pt>, accessed on 7 August 2024), funded by the Foundation for Science and Technology (FCT) and the European Regional Development Fund (FEDER) through LISBOA2020 and ALENTEJO2020 regional operational programmes, in the framework of the National Roadmap of Research Infrastructures of strategic relevance (PINFRA/22128/2016). This study received further support from the FCT (<https://doi.org/10.54499/UIDB/04292/2020>, accessed on 5 August 2024, <https://doi.org/10.54499/UIDB/00006/2020>, accessed on 7 August 2024) awarded to the MARE-Marine and Environmental Sciences Centre through the Associate Laboratory ARNET (<https://doi.org/10.54499/LA/P/0069/2020>, accessed on 7 August 2024). L.F. received support from the National Council for Scientific and Technological Development (CNPq) Brazil (200589/2019-9). A.C.B. was also partially funded by the Scientific Stimulus Programme (CEECIND/00095/2017) of the FCT.

Data Availability Statement: The data presented in this study, collected under the scope of the AQUIMAR project (<https://aquimar.hidrografico.pt/>, accessed on 7 August 2024), are described in the SeaDataNet database of Pan-European infrastructure for ocean and marine data management at <https://www.seadatanet.org/Metadata/CSR-Cruises> (accessed on 7 August 2024), reference numbers 21025541, 21025539, 21025536, and 21025538. Access to the database is subject to request.

Acknowledgments: The authors are also indebted to the ESA Ocean Colour-Climate Change Initiative (OC-CCI) project (<https://climate.esa.int/en/projects/ocean-colour> and <https://www.oceancolour.org>, accessed on 5 August 2024).

Conflicts of Interest: The authors declare no conflicts of interest.

References

1. GCOS. *Systematic Observation Requirements for Satellite-Based Data Products for Climate (2011 Update), Supplemental Details to the Satellite-Based Component of the “Implementation Plan for the Global Observing System for Climate in Support of the UNFCCC (2010 Update)”*; World Meteorological Organization: Geneva, Switzerland, 2011.
2. GCOS. *The Global Observing System for Climate: Implementation Needs*; Global Climate Observing System (GCOS): Geneva, Switzerland, 2016. [CrossRef]
3. Dupouy, C.; Neveux, J.; Ouillon, S.; Frouin, R.; Murakami, H.; Hochard, S.; Dirberg, G. Inherent Optical Properties and Satellite Retrieval of Chlorophyll Concentration in the Lagoon and Open Ocean Waters of New Caledonia. *Mar. Pollut. Bull.* **2010**, *61*, 503–518. [CrossRef] [PubMed]
4. Mobley, C.D. Radiative Transfer in the Ocean. *Encycl. Ocean. Sci.* **2001**, *4*, 2321–2330. [CrossRef]
5. IOCCG. *Atmospheric Correction for Remotely-Sensed Ocean-Colour Products*; Wang, M., Ed.; Reports of the International Ocean-Colour Coordinating Group, No. 10; IOCCG: Dartmouth, NS, Canada, 2010.
6. Kämpf, J.; Chapman, P. The Canary/Iberia Current Upwelling System. In *Upwelling Systems of the World*; Springer: Cham, Switzerland, 2016; pp. 203–250. [CrossRef]
7. Morel, A.; Prieur, L. Analysis of Variations in Ocean Color. *Limnol. Oceanogr.* **1977**, *22*, 709–722. [CrossRef]
8. Wozniak, B.; Wozniak, S.; Tyszka, K.; Dera, J. Modelling the light absorption properties of particulate matter forming organic particles suspended in seawater. Part 1. Model description, classification of organic particles, and example spectra of the light absorption coefficient and the imaginary part of the refractive index of particulate matter for phytoplankton cells and phytoplankton-like particles. *Oceanologia* **2005**, *47*, 129–164.
9. Sathyendranath, S.; Watts, L.; Devred, E.; Platt, T.; Caverhill, C.; Maass, H. Discrimination of Diatoms from Other Phytoplankton Using Ocean-Colour Data. *Mar. Ecol. Prog. Ser.* **2004**, *272*, 59–68. [CrossRef]

10. Alvain, S.; Moulin, C.; Dandonneau, Y.; Bréon, F.M. Remote Sensing of Phytoplankton Groups in Case 1 Waters from Global SeaWiFS Imagery. *Deep Sea Res. Part I Oceanogr. Res. Pap.* **2005**, *52*, 1989–2004. [[CrossRef](#)]
11. Ciotti, A.M.; Bricaud, A. Retrievals of a Size Parameter for Phytoplankton and Spectral Light Absorption by Colored Detrital Matter from Water-Leaving Radiances at SeaWiFS Channels in a Continental Shelf Region off Brazil. *Limnol. Oceanogr. Methods* **2006**, *4*, 237–253. [[CrossRef](#)]
12. Kostadinov, T.S.; Siegel, D.A.; Maritorea, S. Retrieval of the Particle Size Distribution from Satellite Ocean Color Observations. *J. Geophys. Res.* **2009**, *114*, C09015. [[CrossRef](#)]
13. Devred, E.; Sathyendranath, S.; Stuart, V.; Platt, T.A. Three Component Classification of Phytoplankton Absorption Spectra: Application to Ocean-Color Data. *Remote Sens. Environ.* **2011**, *115*, 2255–2266. [[CrossRef](#)]
14. Kostadinov, T.S.; Siegel, D.A.; Maritorea, S. Global Variability of Phytoplankton Functional Types from Space: Assessment via the Particle Size Distribution. *Biogeosciences* **2010**, *7*, 3239–3257. [[CrossRef](#)]
15. Brewin, R.J.W.; Hirata, T.; Hardman-Mountford, N.J.; Lavender, S.J.; Sathyendranath, S.; Barlow, R. The Influence of the Indian Ocean Dipole on Interannual Variations in Phytoplankton Size Structure as Revealed by Earth Observation. *Deep. Sea Res. Part II Top. Stud. Oceanogr.* **2012**, *77–80*, 117–127. [[CrossRef](#)]
16. Goela, P.C.; Icelly, J.; Cristina, S.; Newton, A.; Moore, G.; Cordeiro, C. Specific Absorption Coefficient of Phytoplankton off the Southwest Coast of the Iberian Peninsula: A Contribution to Algorithm Development for Ocean Colour Remote Sensing. *Cont. Shelf Res.* **2013**, *52*, 119–132. [[CrossRef](#)]
17. Brito, A.C.; Sá, C.; Brotas, V.; Brewin, R.J.W.; Silva, T.; Vitorino, J.; Platt, T.; Sathyendranath, S. Effect of Phytoplankton Size Classes on Bio-Optical Properties of Phytoplankton in the Western Iberian Coast: Application of Models. *Remote Sens. Environ.* **2015**, *156*, 537–550. [[CrossRef](#)]
18. Fiúza, A.F.G. Upwelling Patterns off Portugal. In *Coastal Upwelling Its Sediment Record*; Springer: Boston, MA, USA, 1983; pp. 85–98. [[CrossRef](#)]
19. Relvas, P.; Barton, E.D.; Dubert, J.; Oliveira, P.B.; Peliz, Á.; da Silva, J.C.B.; Santos, A.M.P. Physical Oceanography of the Western Iberia Ecosystem: Latest Views and Challenges. *Prog. Oceanogr.* **2007**, *74*, 149–173. [[CrossRef](#)]
20. Ferreira, A.; Dias, J.; Brotas, V.; Brito, A.C. A Perfect Storm: An Anomalous Offshore Phytoplankton Bloom Event in the NE Atlantic (March 2009). *Sci. Total Environ.* **2022**, *806*, 151253. [[CrossRef](#)]
21. Alvarez, I.; Gomez-Gesteira, M.; DeCastro, M.; Lorenzo, M.N.; Crespo, A.J.C.; Dias, J.M. Comparative Analysis of Upwelling Influence between the Western and Northern Coast of the Iberian Peninsula. *Cont. Shelf Res.* **2011**, *31*, 388–399. [[CrossRef](#)]
22. Favareto, L.; Brotas, V.; Rudorff, N.; Zacarias, N.; Tracana, A.; Lamas, L.; Nascimento, Â.; Ferreira, A.; Gomes, M.; Borges, C.; et al. Response of Phytoplankton to Coastal Upwelling: The Importance of Temporal and Spatial Scales. *Limnol. Oceanogr.* **2023**, *68*, 1376–1387. [[CrossRef](#)]
23. Bode, A.; Álvarez, M.; Ruiz-Villarreal, M.; Varela, M.M. Changes in Phytoplankton Production and Upwelling Intensity off A Coruña (NW Spain) for the Last 28 Years. *Ocean Dyn.* **2019**, *69*, 861–873. [[CrossRef](#)]
24. Ferreira, A.; Garrido-Amador, P.; Brito, A.C. Disentangling Environmental Drivers of Phytoplankton Biomass off Western Iberia. *Front. Mar. Sci.* **2019**, *6*, 44. [[CrossRef](#)]
25. GEBCO Bathymetric Compilation Group. *The GEBCO_2021 Grid—A Continuous Terrain Model of the Global Oceans and Land*; British Oceanographic Data Centre NOC: Southampton, UK, 2021. [[CrossRef](#)]
26. Biguino, B.; Olmedo, E.; Ferreira, A.; Zacarias, N.; Lamas, L.; Favareto, L.; Palma, C.; Borges, C.; Teles-Machado, A.; Dias, J.; et al. Evaluation of SMOS L4 Sea Surface Salinity Product in the Western Iberian Coast. *Remote Sens.* **2022**, *14*, 423. [[CrossRef](#)]
27. Zapata, M.; Garrido, J.L. Influence of Injection Conditions in Reversed-Phase High-Performance Liquid Chromatography of Chlorophylls and Carotenoids. *Chromatographia* **1991**, *31*, 589–594. [[CrossRef](#)]
28. Zapata, M.; Rodríguez, F.; Garrido, J. Separation of Chlorophylls and Carotenoids from Marine Phytoplankton: A New HPLC Method Using a Reversed Phase C8 Column and Pyridine-Containing Mobile Phases. *Mar. Ecol. Prog. Ser.* **2000**, *195*, 29–45. [[CrossRef](#)]
29. Mendes, C.R.; Cartaxana, P.; Brotas, V. HPLC Determination of Phytoplankton and Microphytobenthos Pigments: Comparing Resolution and Sensitivity of a C18 and a C8 Method. *Limnol. Oceanogr. Methods* **2007**, *5*, 363–370. [[CrossRef](#)]
30. Cartaxana, P.; Mendes, C.R.; Brotas, V. The COUL method. In *The Fifth SeaWiFS HPLC Analysis Round-Robin Experiment (SeaHARRE-5)*; NASA Tech. Memo, 2012. 2012-217503; NASA Goddard Space Flight Center: Greenbelt, MD, USA, 2012.
31. Brotas, V.; Tarran, G.A.; Veloso, V.; Brewin, R.J.W.; Woodward, E.M.S.; Airs, R.; Beltran, C.; Ferreira, A.; Groom, S.B. Complementary Approaches to Assess Phytoplankton Groups and Size Classes on a Long Transect in the Atlantic Ocean. *Front. Mar. Sci.* **2022**, *8*, 682621. [[CrossRef](#)]
32. Doerffer, R. *Protocols for the Validation of MERIS Water Products*; Document No. PO-TN-MEL-GS-0043; European Space Agency: Paris, France, 2002.
33. Aiken, J.; Pradhan, Y.; Barlow, R.; Lavender, S.; Poulton, A.; Holligan, P.; Hardman-Mountford, N. Phytoplankton Pigments and Functional Types in the Atlantic Ocean: A Decadal Assessment, 1995–2005. *Deep. Sea Res. Part II Top. Stud. Oceanogr.* **2009**, *56*, 899–917. [[CrossRef](#)]

34. Mitchell, B.G.; Kahru, M.; Wieland, J.; Stramska, M. Determination of spectral absorption coefficients of particles, dissolved material and phytoplankton for discrete water samples. In *Ocean Optics Protocols for Satellite Ocean Color Sensor Validation, Revision 4*; National Aeronautical and Space Administration, Goddard Space Flight Center, NASA: Greenbelt, MD, USA, 2003; Chapter 4; Volume 4, pp. 39–60.
35. IOCCG. *IOCCG Ocean Optics and Biogeochemistry Protocols for Satellite Ocean Colour Sensor Validation—Inherent Optical Property Measurements and Protocols: Absorption Coefficient*; Neeley, A.R., Mannino, A., Eds.; International Ocean-Colour Coordinating Group (IOCCG): Dartmouth, NS, Canada, 2018; Volume 1.0, 78p. [[CrossRef](#)]
36. Tassan, S.; Ferrari, G.M. An Alternative Approach to Absorption Measurements of Aquatic Particles Retained on Filters. *Limnol. Oceanogr.* **1995**, *40*, 1358–1368. [[CrossRef](#)]
37. Tassan, S. A Sensitivity Analysis of the ‘Transmittance-Reflectance’ Method for Measuring Light Absorption by Aquatic Particles. *J. Plankton Res.* **2002**, *24*, 757–774. [[CrossRef](#)]
38. Stramski, D.; Reynolds, R.A.; Kaczmarek, S.; Uitz, J.; Zheng, G. Correction of Pathlength Amplification in the Filter-Pad Technique for Measurements of Particulate Absorption Coefficient in the Visible Spectral Region. *Appl. Opt.* **2015**, *54*, 6763. [[CrossRef](#)]
39. Pope, R.M.; Fry, E.S. Absorption Spectrum (380–700 Nm) of Pure Water II Integrating Cavity Measurements. *Appl. Opt.* **1997**, *36*, 8710. [[CrossRef](#)]
40. Bricaud, A.; Morel, A.; Prieur, L. Absorption by Dissolved Organic Matter of the Sea (Yellow Substance) in the UV and Visible Domains1. *Limnol. Oceanogr.* **1981**, *26*, 43–53. [[CrossRef](#)]
41. Babin, M.; Stramski, D.; Ferrari, G.M.; Claustre, H.; Bricaud, A.; Obolensky, G.; Hoepffner, N. Variations in the Light Absorption Coefficients of Phytoplankton, Nonalgal Particles, and Dissolved Organic Matter in Coastal Waters around Europe. *J. Geophys. Res.* **2003**, *108*, 3211. [[CrossRef](#)]
42. Bricaud, A.; Babin, M.; Claustre, H.; Ras, J.; Tièche, F. Light Absorption Properties and Absorption Budget of Southeast Pacific Waters. *J. Geophys. Res.* **2010**, *115*, C08009. [[CrossRef](#)]
43. Matsuoka, A.; Bricaud, A.; Benner, R.; Para, J.; Sempéré, R.; Prieur, L.; Bélanger, S.; Babin, M. Tracing the Transport of Colored Dissolved Organic Matter in Water Masses of the Southern Beaufort Sea: Relationship with Hydrographic Characteristics. *Biogeosciences* **2012**, *9*, 925–940. [[CrossRef](#)]
44. Sathyendranath, S.; Brewin, R.; Brockmann, C.; Brotas, V.; Calton, B.; Chuprin, A.; Cipollini, P.; Couto, A.; Dingle, J.; Doerffer, R.; et al. An Ocean-Colour Time Series for Use in Climate Studies: The Experience of the Ocean-Colour Climate Change Initiative (OC-CCI). *Sensors* **2019**, *19*, 4285. [[CrossRef](#)] [[PubMed](#)]
45. Gohin, F.; Druon, J.N.; Lampert, L. A Five Channel Chlorophyll Concentration Algorithm Applied to SeaWiFS Data Processed by SeaDAS in Coastal Waters. *Int. J. Remote Sens.* **2002**, *23*, 1639–1661. [[CrossRef](#)]
46. Brotas, V.; Brewin, R.J.W.; Sá, C.; Brito, A.C.; Silva, A.; Mendes, C.R.; Diniz, T.; Kaufmann, M.; Tarran, G.; Groom, S.B.; et al. Deriving Phytoplankton Size Classes from Satellite Data: Validation along a Trophic Gradient in the Eastern Atlantic Ocean. *Remote Sens. Environ.* **2013**, *134*, 66–77. [[CrossRef](#)]
47. Maritorea, S.; Siegel, D.A.; Peterson, A.R. Optimization of a Semianalytical Ocean Color Model for Global-Scale Applications. *Appl. Opt.* **2002**, *41*, 2705. [[CrossRef](#)]
48. Lee, Z.; Carder, K.L.; Arnone, R.A. Deriving Inherent Optical Properties from Water Color: A Multiband Quasi-Analytical Algorithm for Optically Deep Waters. *Appl. Opt.* **2002**, *41*, 5755. [[CrossRef](#)]
49. Werdell, P.J.; Franz, B.A.; Bailey, S.W.; Feldman, G.C.; Boss, E.; Brandt, V.E.; Dowell, M.; Hirata, T.; Lavender, S.J.; Lee, Z.; et al. Generalized Ocean Color Inversion Model for Retrieving Marine Inherent Optical Properties. *Appl. Opt.* **2013**, *52*, 2019. [[CrossRef](#)]
50. Bricaud, A.; Morel, A.; Babin, M.; Allali, K.; Claustre, H. Variations of Light Absorption by Suspended Particles with Chlorophyll a Concentration in Oceanic (Case 1) Waters: Analysis and Implications for Bio-optical Models. *J. Geophys. Res.* **1998**, *103*, 31033–31044. [[CrossRef](#)]
51. Bricaud, A.; Babin, M.; Morel, A.; Claustre, H. Variability in the Chlorophyll-specific Absorption Coefficients of Natural Phytoplankton: Analysis and Parameterization. *J. Geophys. Res.* **1995**, *100*, 13321–13332. [[CrossRef](#)]
52. Sá, C.; D’Alimonte, D.; Brito, A.C.; Kajiyama, T.; Mendes, C.R.; Vitorino, J.; Oliveira, P.B.; da Silva, J.C.B.; Brotas, V. Validation of Standard and Alternative Satellite Ocean-Color Chlorophyll Products off Western Iberia. *Remote Sens. Environ.* **2015**, *168*, 403–419. [[CrossRef](#)]
53. Bailey, S.W.; Werdell, P.J. A Multi-Sensor Approach for the on-Orbit Validation of Ocean Color Satellite Data Products. *Remote Sens. Environ.* **2006**, *102*, 12–23. [[CrossRef](#)]
54. Seegers, B.N.; Stumpf, R.P.; Schaeffer, B.A.; Loftin, K.A.; Werdell, P.J. Performance Metrics for the Assessment of Satellite Data Products: An Ocean Color Case Study. *Opt. Express* **2018**, *26*, 7404. [[CrossRef](#)] [[PubMed](#)]
55. Bisson, K.; Werdell, P.; Chase, A.; Kramer, S.; Cael, B.; Boss, E.; McKinna, L.; Behrenfeld, M. Informing Ocean Color Inversion Products by Seeding with Ancillary Observations. *Opt. Express* **2023**, *31*, 40557. [[CrossRef](#)]
56. Loisel, H.; Lubac, B.; Dessailly, D.; Duforet-Gaurier, L.; Vantrepotte, V. Effect of Inherent Optical Properties Variability on the Chlorophyll Retrieval from Ocean Color Remote Sensing: An in Situ Approach. *Opt. Express* **2010**, *18*, 20949. [[CrossRef](#)]
57. Morel, A.; Antoine, D. Algorithm Theoretical Basis Document 2.9: Pigment Index Retrieval in Case 1 Waters. 2011. Available online: https://earth.esa.int/eogateway/documents/20142/37627/MERIS_ATBD_2.9_v4.3++2011.pdf/e03662c8-7b57-fb00-f6c7-46f5a950c4be (accessed on 5 August 2024).

58. Bricaud, A.; Claustre, H.; Ras, J.; Oubelkheir, K. Natural Variability of Phytoplanktonic Absorption in Oceanic Waters: Influence of the Size Structure of Algal Populations. *J. Geophys. Res.* **2004**, *109*, C11010. [CrossRef]
59. Doerffer, R.; Schiller, H. The MERIS Case 2 Water Algorithm. *Int. J. Remote Sens.* **2007**, *28*, 517–535. [CrossRef]
60. Antoine, D.; Bourq, L.; Brockmann, C.; Doerffer, R.; Fischer, J.; Moore, J.; Santer, R.; Zagolski, F. Reference Model for MERIS Level 2 Processing—Third MERIS reprocessing: Ocean Branch, Report n. PO-TN-MEL-GS-0026-5 Rev. 2. 2012. Available online: <http://envisat.esa.int/instruments/meris/rfm/> (accessed on 5 August 2024).
61. Peliz, Á.; Rosa, T.L.; Santos, A.M.P.; Pissarra, J.L. Fronts, Jets, and Counter-Flows in the Western Iberian Upwelling System. *J. Mar. Syst.* **2002**, *35*, 61–77. [CrossRef]
62. Vantrepotte, V.; Brunet, C.; Mériaux, X.; Lécuyer, E.; Vellucci, V.; Santer, R. Bio-Optical Properties of Coastal Waters in the Eastern English Channel. *Estuar. Coast. Shelf Sci.* **2007**, *72*, 201–212. [CrossRef]
63. Valente, A.; da Silva, J.C.B.; Brotas, V. Linking Ocean Colour Features in the Western Iberian Margin to Wave-Induced Sediment Resuspension and Coccolithophore Patches. *Cont. Shelf Res.* **2021**, *225*, 104482. [CrossRef]
64. Quaresma, L.S.; Vitorino, J.; Oliveira, A.; da Silva, J. Evidence of Sediment Resuspension by Nonlinear Internal Waves on the Western Portuguese Mid-Shelf. *Mar. Geol.* **2007**, *246*, 123–143. [CrossRef]
65. Sá, C.G.V. Ocean Colour off the Portuguese Coast: Chlorophyll α Products Validation and Applicability. Ph.D. Thesis, Marine Sciences, University of Lisbon, Faculty of Sciences, Lisbon, Portugal, October 2013.
66. Helms, J.R.; Stubbins, A.; Ritchie, J.D.; Minor, E.C.; Kieber, D.J.; Mopper, K. Absorption Spectral Slopes and Slope Ratios as Indicators of Molecular Weight, Source, and Photobleaching of Chromophoric Dissolved Organic Matter. *Limnol. Oceanogr.* **2008**, *53*, 955–969. [CrossRef]
67. Goela, P.C.; Icely, J.; Cristina, S.; Danchenko, S.; Angel DelValls, T.; Newton, A. Using Bio-Optical Parameters as a Tool for Detecting Changes in the Phytoplankton Community (SW Portugal). *Estuar. Coast. Shelf Sci.* **2015**, *167*, 125–137. [CrossRef]
68. Mendes, C.R.; Sá, C.; Vitorino, J.; Borges, C.; Tavano Garcia, V.M.; Brotas, V. Spatial Distribution of Phytoplankton Assemblages in the Nazaré Submarine Canyon Region (Portugal): HPLC-CHEMTAX Approach. *J. Mar. Syst.* **2011**, *87*, 90–101. [CrossRef]
69. Moita, M.T. Structure, Variability and Dynamics of Phytoplankton from the Portuguese Continental Coast. Ph.D. Thesis, University of Lisbon, Lisbon, Portugal, 2001.
70. Silva, A.; Palma, S.; Oliveira, P.B.; Moita, M.T. Composition and Interannual Variability of Phytoplankton in a Coastal Upwelling Region (Lisbon Bay, Portugal). *J. Sea Res.* **2009**, *62*, 238–249. [CrossRef]
71. Sousa, M.C.; deCastro, M.; Alvarez, I.; Gomez-Gesteira, M.; Dias, J.M. Why Coastal Upwelling Is Expected to Increase along the Western Iberian Peninsula over the next Century? *Sci. Total Environ.* **2017**, *592*, 243–251. [CrossRef]
72. Duyens, L.N.M. The Flattering of the Absorption Spectrum of Suspensions, as Compared to That of Solutions. *Biochim. Biophys. Acta* **1956**, *19*, 1–12. [CrossRef]
73. Tilstone, G.; Mallor-Hoya, S.; Gohin, F.; Couto, A.B.; Sá, C.; Goela, P.; Cristina, S.; Airs, R.; Icely, J.; Zühlke, M.; et al. Which Ocean Colour Algorithm for MERIS in North West European Waters? *Remote Sens. Environ.* **2017**, *189*, 132–151. [CrossRef]
74. Bricaud, A.; Ciotti, A.M.; Gentili, B. Spatial-temporal Variations in Phytoplankton Size and Colored Detrital Matter Absorption at Global and Regional Scales, as Derived from Twelve Years of SeaWiFS Data (1998–2009). *Glob. Biogeochem. Cycles* **2012**, *26*, GB1010. [CrossRef]
75. Reynolds, R.A.; Stramski, D.; Mitchell, B.G. A Chlorophyll-dependent Semianalytical Reflectance Model Derived from Field Measurements of Absorption and Backscattering Coefficients within the Southern Ocean. *J. Geophys. Res.* **2001**, *106*, 7125–7138. [CrossRef]
76. Chen, J.; Zhu, W.; Tian, Y.Q.; Yu, Q.; Zheng, Y.; Huang, L. Remote Estimation of Colored Dissolved Organic Matter and Chlorophyll-a in Lake Huron Using Sentinel-2 Measurements. *J. Appl. Remote Sens.* **2017**, *11*, 036007. [CrossRef]
77. Mannino, A.; Russ, M.E.; Hooker, S.B. Algorithm Development and Validation for Satellite-derived Distributions of DOC and CDOM in the U.S. Middle Atlantic Bight. *J. Geophys. Res.* **2008**, *113*, C07051. [CrossRef]
78. Gohin, F. Annual cycles of chlorophyll-a, non-algal suspended particulate matter, and turbidity observed from space and in-situ in coastal waters. *Ocean Sci.* **2011**, *7*, 705–732. [CrossRef]
79. O'Reilly, J.E.; Maritorena, S.; Siegel, D.A.; O'Brien, M.C.; Toole, D.; Mitchell, B.G.; Kahru, M.; Chavez, F.P.; Strutton, P.; Cota, G.F.; et al. *Ocean Color Chlorophyll a Algorithms for SeaWiFS, OC2, OC4: Version 4*; Volume 11 of SeaWiFS Postlaunch Technical Report Series NASA/TM-1995-104566; NASA Goddard Space Flight Center: Greenbelt, MD, USA, 2000; pp. 9–23.
80. Lee, Z.; Arnone, R.; Hu, C.; Werdell, P.J.; Lubac, B. Uncertainties of Optical Parameters and Their Propagations in an Analytical Ocean Color Inversion Algorithm. *Appl. Opt.* **2010**, *49*, 369. [CrossRef] [PubMed]
81. Lee, Z.; Lance, V.P.; Shang, S.; Vaillancourt, R.; Freeman, S.; Lubac, B.; Hargreaves, B.R.; Del Castillo, C.; Miller, R.; Twardowski, M.; et al. An Assessment of Optical Properties and Primary Production Derived from Remote Sensing in the Southern Ocean (SO GasEx). *J. Geophys. Res.* **2011**, *116*, C00F03. [CrossRef]
82. Clay, S.; Peña, A.; DeTracey, B.; Devred, E. Evaluation of Satellite-Based Algorithms to Retrieve Chlorophyll-a Concentration in the Canadian Atlantic and Pacific Oceans. *Remote Sens.* **2019**, *11*, 2609. [CrossRef]
83. Werdell, P.J.; McKinna, L.I.W.; Boss, E.; Ackleson, S.G.; Craig, S.E.; Gregg, W.W.; Lee, Z.; Maritorena, S.; Roesler, C.S.; Rousseaux, C.S.; et al. An Overview of Approaches and Challenges for Retrieving Marine Inherent Optical Properties from Ocean Color Remote Sensing. *Prog. Oceanogr.* **2018**, *160*, 186–212. [CrossRef]

84. Garcia, R.A.; Lee, Z.; Hochberg, E.J. Hyperspectral Shallow-Water Remote Sensing with an Enhanced Benthic Classifier. *Remote Sens.* **2018**, *10*, 147. [[CrossRef](#)]
85. Wei, J.; Lee, Z.; Shang, S.; Yu, X. Semianalytical Derivation of Phytoplankton, CDOM, and Detritus Absorption Coefficients from the Landsat 8/OLI Reflectance in Coastal Waters. *JGR Ocean.* **2019**, *124*, 3682–3699. [[CrossRef](#)]
86. Zheng, G.; DiGiacomo, P.M. Uncertainties and Applications of Satellite-Derived Coastal Water Quality Products. *Prog. Oceanogr.* **2017**, *159*, 45–72. [[CrossRef](#)]
87. Najah, A.; Al-Shehhi, M.R. Performance of the Ocean Color Algorithms: QAA, GSM, and GIOP in Inland and Coastal Waters. *Remote Sens. Earth Syst. Sci.* **2021**, *4*, 235–248. [[CrossRef](#)]
88. O’Shea, R.E.; Pahlevan, N.; Smith, B.; Boss, E.; Gurlin, D.; Alikas, K.; Kangro, K.; Kudela, R.M.; Vaičiūtė, D. A Hyperspectral Inversion Framework for Estimating Absorbing Inherent Optical Properties and Biogeochemical Parameters in Inland and Coastal Waters. *Remote Sens. Environ.* **2023**, *295*, 113706. [[CrossRef](#)]

Disclaimer/Publisher’s Note: The statements, opinions and data contained in all publications are solely those of the individual author(s) and contributor(s) and not of MDPI and/or the editor(s). MDPI and/or the editor(s) disclaim responsibility for any injury to people or property resulting from any ideas, methods, instructions or products referred to in the content.